Arc mediates intercellular synaptic plasticity via IRSp53-dependent extracellular vesicle biogenesis.

Alicia Ravens[1,*], Kaelan Sullivan[1,*], Jenifer Einstein[1], Sevnur Kömürlü Keceli [2], Tom Kicmal[2], Mitali Tyagi[1], Michael P. Hantak[1], Tate Shepherd[1], Alyson Stewart[1], Kenneth Lyon[1], Adarsh Dharan[2], Thomas Gallagher[2], Edward M. Campbell[2], Jason D. Shepherd[1, #].

[1]Department of Neurobiology, University of Utah.

[2]Department of Microbiology and Immunology, Stritch School of Medicine, Loyola University Chicago.

[#]Lead Contact: Jason.Shepherd@neuro.utah.edu

* Equal contribution

Abstract

Current models of learning and memory have focused on cell-autonomous regulation of synaptic strength; however, intercellular signaling between cells in the brain is critical for normal cognition. The immediate early gene *Arc* is a repurposed retrotransposon critical for long-term forms of synaptic plasticity and memory. Arc protein forms virus-like capsids released in extracellular vesicles (EVs) that signal cell-to-cell. Here, we find that long-term potentiation (LTP) stimuli induce the biogenesis of Arc EVs by recruiting the I-BAR protein IRSp53 to dendrites, which facilitates Arc capsid assembly and release. Arc EVs transfer Arc protein and mRNA to neighboring neurons, where translation of transferred *Arc* mRNA induces a loss of surface AMPA-type glutamate receptors. These results show that Arc EVs mediate non-cell autonomous long-term depression (LTD), revealing an intercellular form of synaptic plasticity that may be critical for memory consolidation.

Introduction

Learning and experience stimulates the expression of a specific set of genes that implement long-lasting changes in neuronal connectivity and synapse strength[1]. The immediate early gene *Arc* is a critical mediator of long-lasting synaptic plasticity and memory[2,3]. Recent studies showed that *Arc* evolved from an ancient retrotransposon and that Arc protein contains conserved structural sequences of the retroviral Gag protein[4-7]. Similar to retroviruses, Arc forms capsids that are released from neurons with an enveloped membrane in extracellular vesicles (EVs), which transfer RNAs and proteins to recipient neurons[6]. However, the function of Arc intercellular signaling is unknown.

Cellular models of synaptic plasticity, such as long-term potentiation and depression (LTP/LTD), have focused on cell-autonomous mechanisms[8]. Arc regulates the endocytosis of AMPA-type glutamate receptors through interactions with endocytic proteins to mediate LTD[9] and homeostatic plasticity[10,11]. However, the expression of Arc is also induced by LTP stimuli[12], despite not being strictly required for LTP expression[13]. EVs are emerging as critical mediators of intercellular signaling in the nervous system[14], and EV release is induced by neuronal activity[15]. However, the role of EVs in synaptic plasticity is unclear. Thus, we set out to determine whether neuronal activity regulates Arc release in EVs and whether Arc intercellular signaling affects synaptic function.

Arc interacts with synaptic proteins, such as PSD-95 and TARP-γ2, through a common binding motif in the N-lobe[7]. Another synaptic protein, IRSp53 (also known as BAIAP2)[16], was predicted to interact with Arc in the same region[7]. Intriguingly, IRSp53 is also critical for HIV-1 capsid release from the plasma membrane[17,18]. IRSp53 is an I-BAR protein that interacts with membranes to induce outward curvature through interactions with the actin machinery via its SH3 domain[19]. IRSp53 has also been shown to induce dendritic spine formation[20] and is associated with psychiatric disorders such as autism and schizophrenia[21]. IRSp53 may also play a role in EV biogenesis, regulating the release of a specific subset of EVs from the plasma membrane in non-neuronal cells[22]. Here, we find that IRSp53 facilitates Arc capsid assembly and Arc EV biogenesis. LTP stimuli induces the formation of Arc-IRSp53 complexes that traffic anterograde in dendrites, which are released from filopodial-like projections. Arc transfer occurs in neighboring dendrites, resulting in a loss of surface AMPA receptors. Arc EVs are sufficient to induce loss of surface AMPARs in recipient neurons, which requires delivery and translation of *Arc* mRNA. Together, these results suggest that Arc mediates a novel form of intercellular synaptic plasticity through LTP-induced IRSp53-dependent release of Arc EVs.

Results

Arc directly binds IRSp53.

IRSp53 is highly expressed in neurons and at synapses[23,24] and has also been implicated in the release of HIV-1 capsids[17]. Since Arc and HIV-1 share structural homology[7], we hypothesized that IRSp53 may play a critical role in Arc release and EV biogenesis. To test if Arc and IRSp53 interact in the brain *in vivo*, we immunoprecipitated (IP) Arc from homogenized brain tissue in 1-month-old mice (Figure 1A) that had experienced six hours of home-cage enrichment to increase Arc expression (Supplementary Figure 1A-D). IRSp53 co-IPs with Arc in brain cortical lysates (Figure 1A). Arc also co-IPs with PSD-95, a known interacting partner[25]. To investigate whether this interaction occurs by direct binding, we performed a Glutathione S-transferase (GST) pulldown assay using purified GST tagged IRSp53 and Arc protein. GST-IRSp53 bound on the column was incubated with purified Arc protein. Both Arc and IRSp53 eluted together in the bound fraction. However, Arc was not found in the eluted fraction when incubated with GST on the column, demonstrating a direct and specific protein-protein interaction (Figure 1B). We next determined the region of Arc required for IRSp53 binding by screening a series of Arc deletion mutants (Supplementary Figure 1E) co-transfected with IRSp53 in HEK293T cells (Supplementary Figure 1F-H). We found that Arc deletion mutants $Arc^{\Delta 1\text{-}45}$ and $Arc^{\Delta 20\text{-}40}$ did not robustly co-IP with IRSp53, suggesting the 20-40 amino acid N-terminal region of Arc is required for binding (Figure 1C, Supplementary Figure 1F). To test whether IRSp53 interacts with the capsid form of Arc, we incubated recombinant purified Arc capsids (see methods) with HEK293T cell lysates obtained from cells transfected with IRSp53 and then pelleted the capsids using ultracentrifugation. IRSp53 pelleted with Arc capsids but did not pellet when Arc capsids were not present (Figure 1D). These results show that Arc and IRSp53 interact in the brain *in vivo* and that this interaction likely occurs through direct binding.

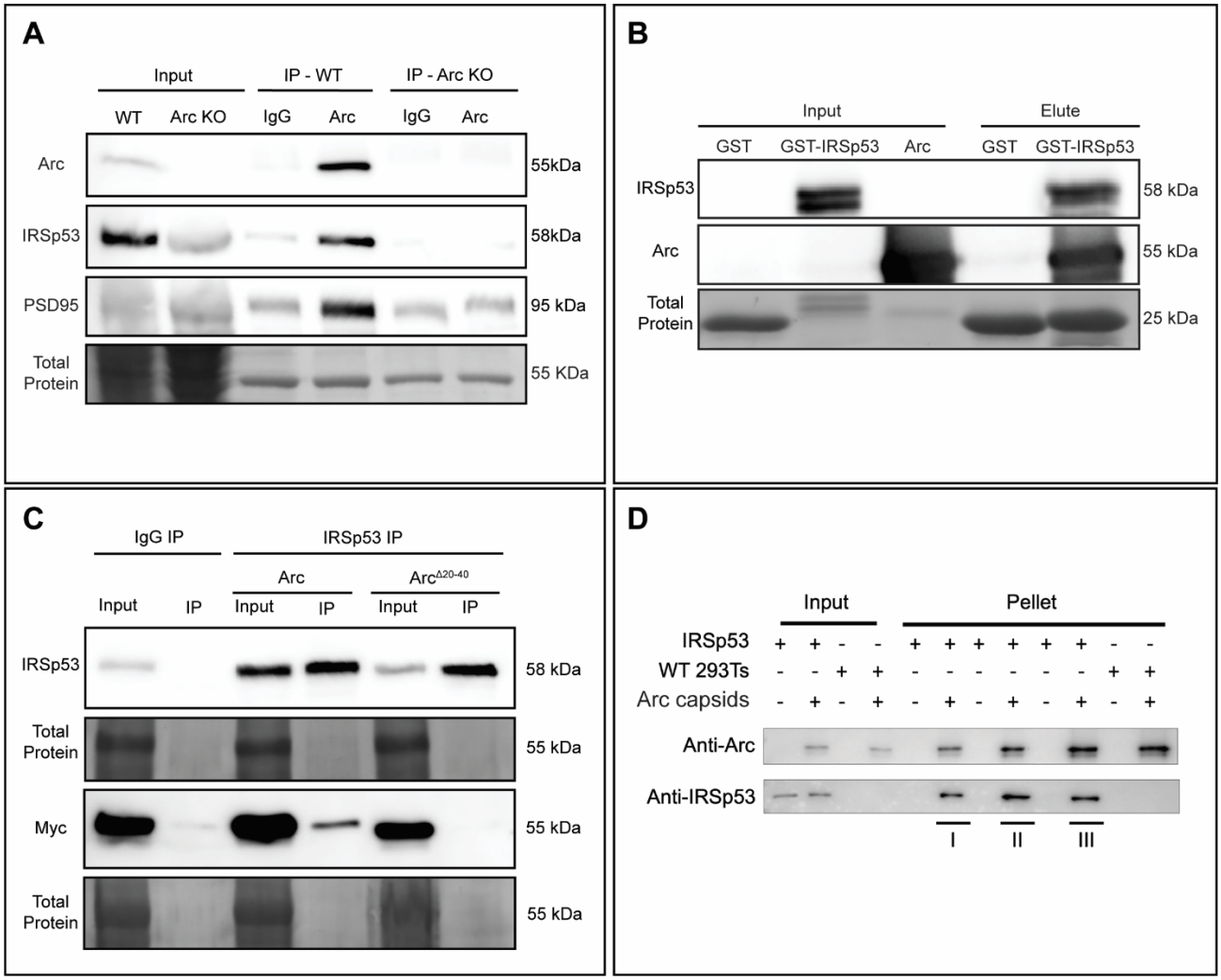

Figure 1. IRSp53 co-immunoprecipitates and directly interacts with Arc. A. *IRSp53 co-IPs with Arc*. Forebrain tissue was collected from 1-month-old WT and Arc KO mice that experienced 6 hours of enriched environment to increase Arc expression and cell lysates were incubated with IgG or Arc antibody. Input and IP samples were blotted for Arc, IRSp53, and PSD-95. **B.** *IRSp53 directly binds to Arc.* Purified GST-IRSp53, bound to column, was incubated with purified Arc protein. A band for Arc is present in the bound IRSp53 fraction. **C.** *Arc$^{\Delta 20\text{-}40}$ does not co-IP with IRSp53*. HEK cells were transfected with IRSp53 and either myc-Arc or myc-Arc$^{\Delta 20\text{-}40}$. Cell lysates were incubated with an IgG or IRSp53 antibody and IP samples were blotted for IRSp53 and myc. **D.** *IRSp53 interacts with Arc capsids*. IRSp53 over-expressing cell lysates were incubated with purified Arc capsids and the mixture was pelleted by ultracentrifugation. Arc capsids were found in the pellet fractions in the presence and absence of IRSp53. IRSp53 protein was found in the pellet only in the presence of Arc capsids. I-III are technical replicates. Data are representative of three biological replicates.

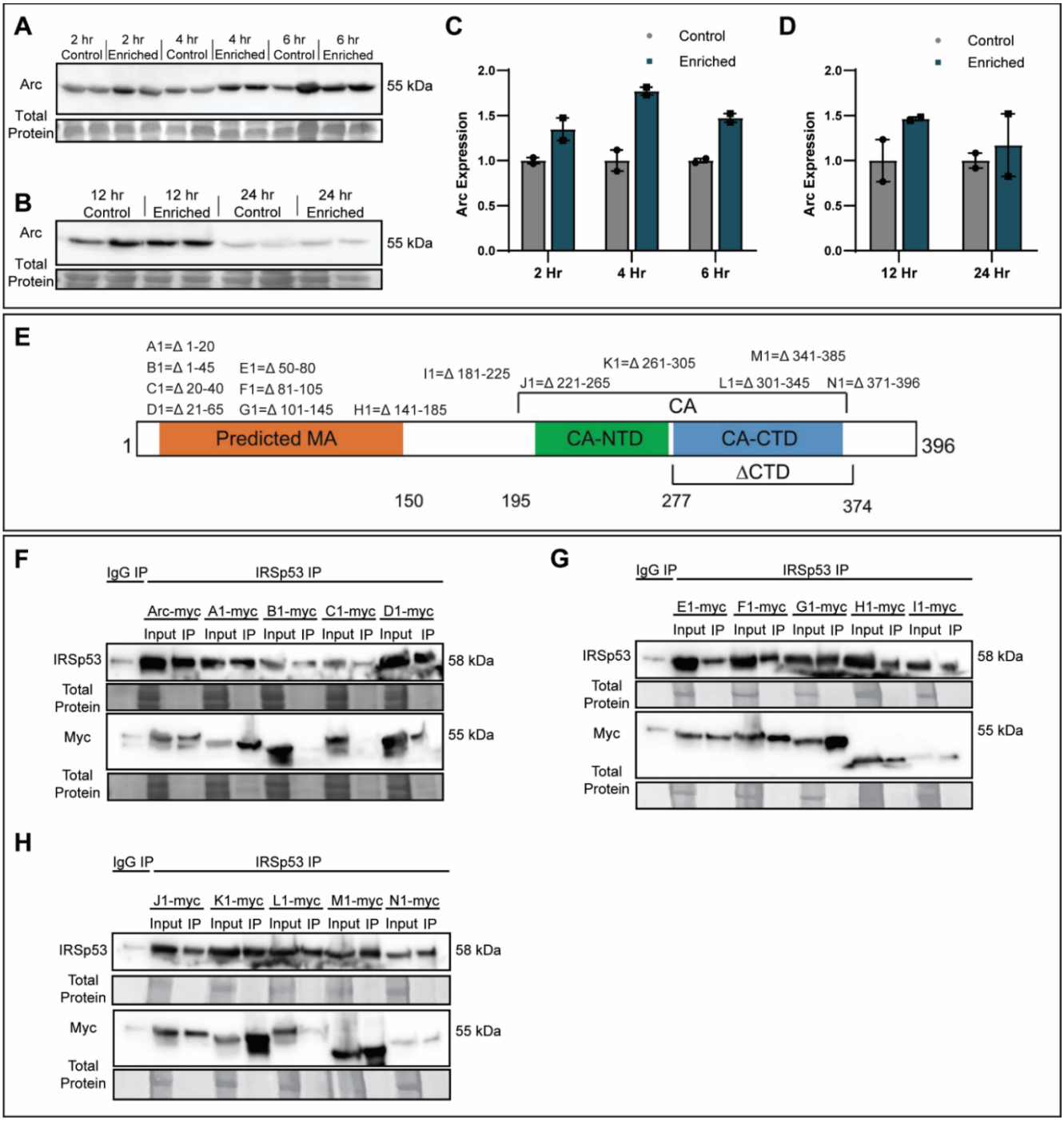

Supplementary Figure 1. Arc is induced by environmental enrichment and co-immunoprecipitates with IRSp53 via an N-terminal region, related to Figure 1. A-B. *Arc expression peaks at 4 hours following home-cage enrichment in the forebrain.* Toys were placed in the home cage of P30 C57BL/6 WT mice at the start of their active cycle. Enrichment toys were left in the cage until animals were sacrificed. Forebrain tissue was collected at 2-, 4-, 6-, 12-, and 24-hours post-enrichment or from unenriched controls (n=2 per group/per timepoint). **C-D.** Quantification of Arc expression in the forebrain following home-cage enrichment (from blots in A and B). Densitometric analysis was performed using FIJI. Arc bands were first normalized to total protein and then to their respective timepoint control. **E.** Schematic depicting the predicted capsid and MA domains of Arc and the deletion mutants screened. **F-H.** *N-terminal Arc deletion mutants do not co-IP with IRSp53.* HEK293T cells were transfected with IRSp53 and myc-Arc or one of the 14 Arc deletion mutants. Cell lysates were collected 48 hours following transfection and incubated with an IgG or IRSp53 antibody. IP samples were blotted for IRSp53, or myc. $Arc^{\Delta 1\text{-}45}$ and $Arc^{\Delta 20\text{-}40}$ do not co-IP with IRSp53.

IRSp53 facilitates Arc capsid assembly.

IRSp53 interacts with Arc capsids, thus we determined whether IRSp53 regulates capsid assembly. We affinity-purified Arc and IRSp53 protein from E. coli for *in vitro* capsid assembly assays. We previously found that high phosphate or salt levels in the buffer are sufficient to drive self-assembly of Arc capsids[6]. To determine whether IRSp53 facilitates Arc capsid assembly, we incubated Arc with IRSp53 in a 1:1 molar ratio in Tris-buffered saline solution (TBS), a buffer not conducive for Arc capsid assembly. We then performed size exclusion chromatography (SEC) on the purified samples and collected the peak protein fractions (Supplementary Figure 2A-B; Fractions 14-16 for Arc, Arc+IRSp53, Arc+GST, IRSp53; fractions 24-26 for GST). 0.5 mg/mL of protein from these fractions was added to grids and processed for negative stain transmission electron microscopy (TEM). Arc capsids in TBS were rarely observed, and no capsid structures were observed on grids with IRSp53 or GST alone (Figure 2A). When GST was incubated with Arc protein in TBS, there was no effect on Arc capsid formation. In contrast, when Arc and IRSp53 were incubated together in TBS, the number of capsids observed was comparable to Arc alone in high phosphate buffer (Figure 2A). These data show that IRSp53 facilitates Arc capsid assembly *in vitro*.

IRSp53 mediates Arc release in EVs.

Retroviruses are released from cells in membrane-enveloped particles and IRSp53 is critical for HIV release[17,18,14]. To test whether IRSp53 facilitates Arc release in EVs, we used a split-nano luciferase system[26]. We cloned the small HiBiT tag (11 amino acids) onto Arc's C-terminus (Figure 2B), which we confirmed does not interfere with capsid formation (Supplemental Figure 2C). We transfected HEK293T cells with Arc-HiBiT alone or Arc-HiBiT+IRSp53. Cell lysate and media samples were collected to measure luciferase luminescence, which occurs after HiBiT complementation with Large-bit (LgBiT) when added to the media (Figure 2B). When IRSp53 is co-expressed with Arc, release is enhanced approximately 20-fold, whereas GFP co-expression had no effect (Figure 2C). To determine whether signal derived from the media containing Arc-HiBiT is enclosed within EVs, we measured luminescence with or without membrane-emulsifying detergent. We find that detergent was required for the majority of HiBiT-LgBiT complementation and luciferase activity, suggesting that Arc-HiBiT is protected within the EV lumen (Figure 2D). To further confirm that IRSp53 enhanced the release of Arc into EVs, we collected media from HEK293T cells transfected with Arc or Arc+IRSp53 and performed SEC or nanoparticle tracking. We find that the Arc protein released when co-expressed with IRSp53 is found in particles that have sizes and densities consistent with EVs (Figure 2E-F). IRSp53 did not facilitate $Arc^{\Delta 20\text{-}40}$ release (Supplementary Figure 2D), consistent with $Arc^{\Delta 20\text{-}40}$ unable to bind IRSp53 (Figure 1C). To gain further insight into how IRSp53 may regulate Arc release, we used a point mutant of the SH3 domain (I403P), which has previously been shown to block downstream interactions with actin machinery proteins such as WAVE2, N-WASP, and Dynamin1[27]. $IRSp53^{I403P}$ does not enhance Arc release in HEK cells (Supplementary Figure 2D) but is still capable of binding to Arc protein and facilitating Arc capsid assembly (Supplemental Figure 2F-G). Furthermore, Endophilin, an N-BAR domain-containing protein known to interact with Arc[9], did not facilitate Arc release from HEK cells (Supplemental Figure 2E). This suggests that Arc release is specifically facilitated by IRSp53 and not all BAR domain-containing proteins.

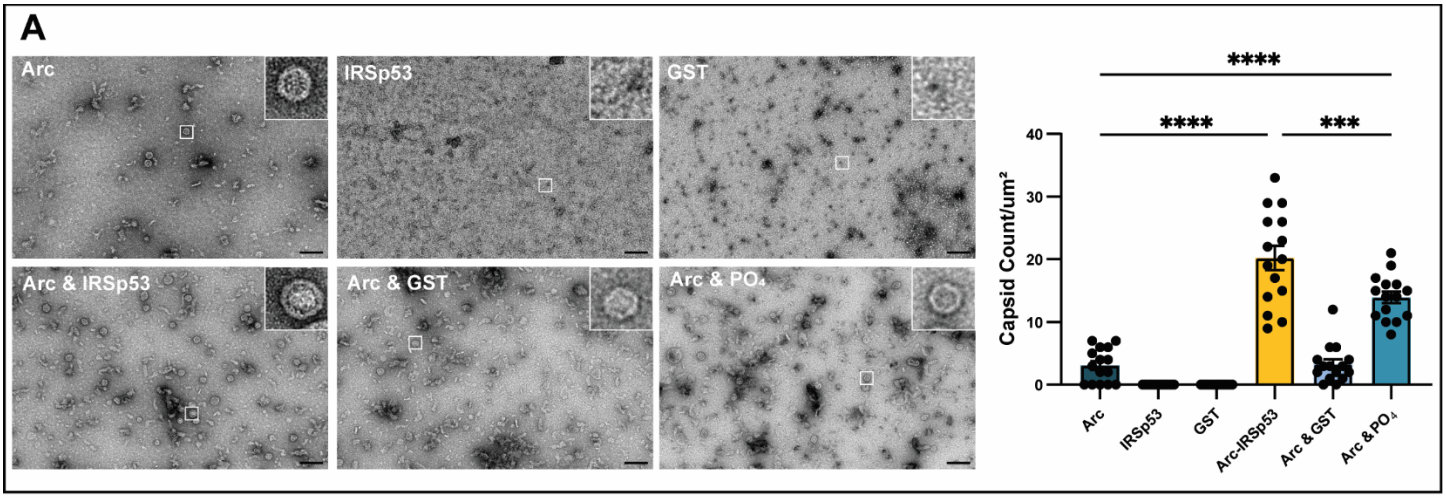

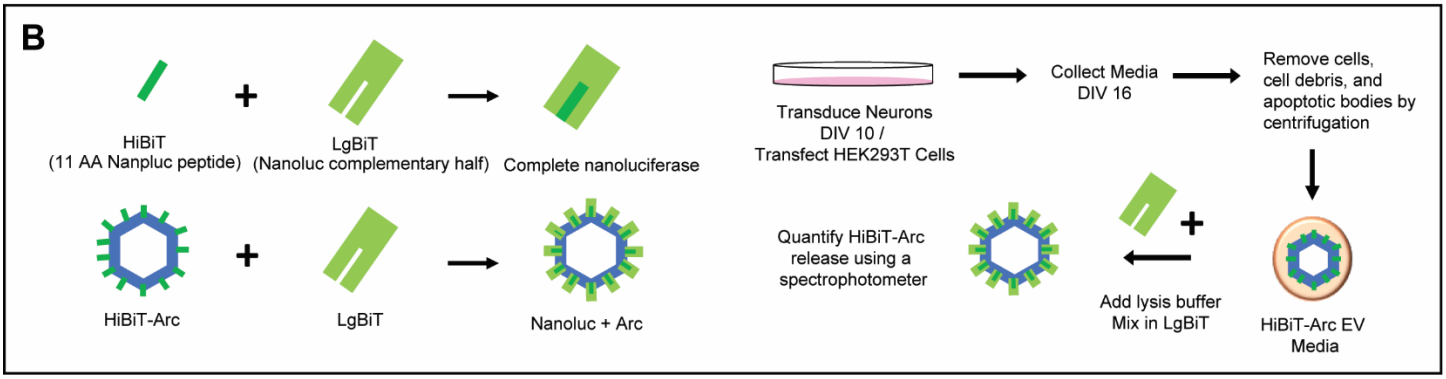

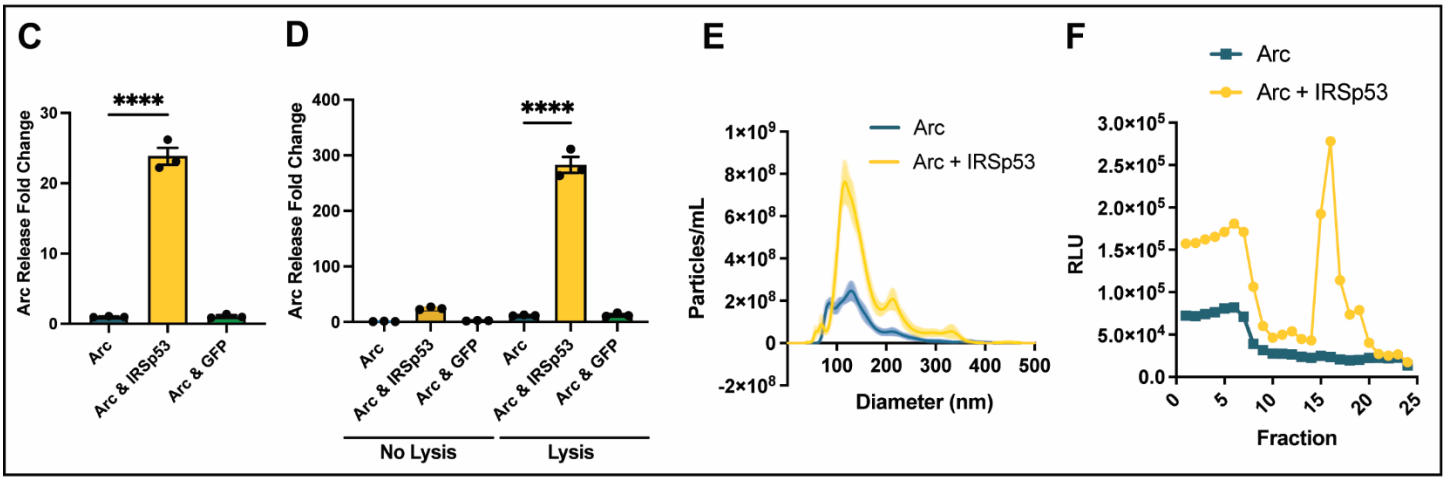

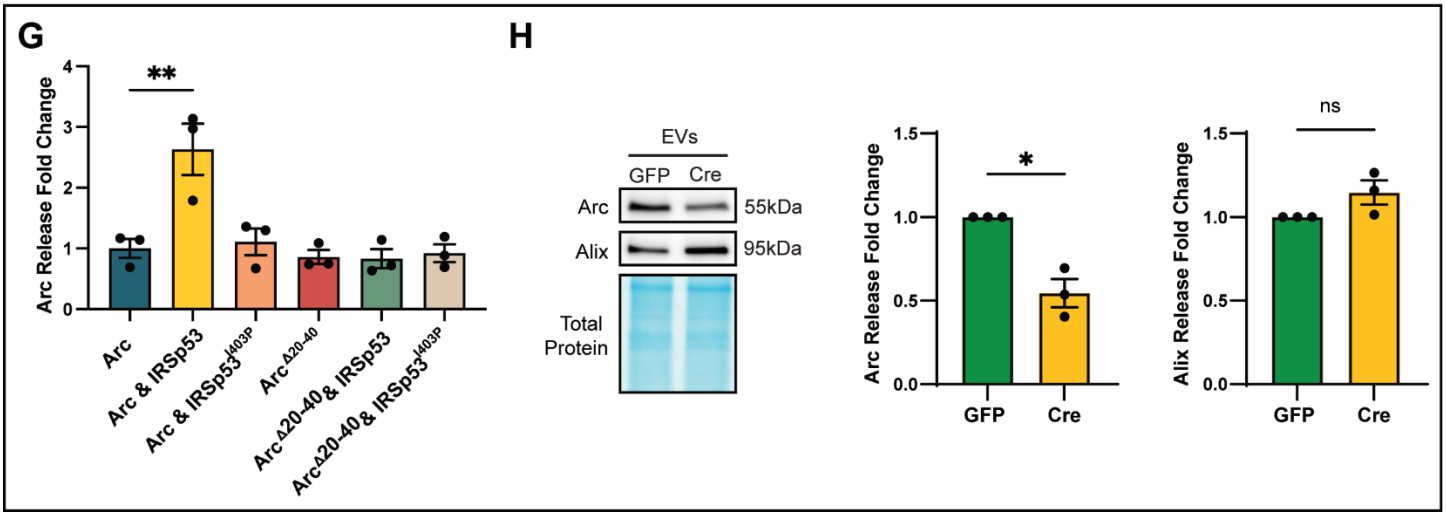

Figure 2. IRSp53 facilitates Arc capsid assembly and release into extracellular vesicles. A. *IRSp53 facilitates Arc capsid assembly.* Representative TEM images of Arc, IRSp53, GST, Arc+IRSp53 (1:1), Arc+GST (1:1) all in TBS buffer, and Arc in 500mM phosphate bufferM, at 0.5mg/m (n=15 images/grid). Scale bar=100nm. Statistics: ***p=0.0003, ****p<0.0001, one-way ANOVA. Data is representative of 3 independent experiments. **B.** *Arc release assay*. HiBiT (11 amino acids) is a split nanoluciferase that complexes with LgBiT to form a complete nanoluciferase. HiBiT is tagged to the C-terminus of Arc. Neurons were transduced on DIV10 with Arc-HiBiT. On DIV16 media was removed, EVs were collected and lysed and purified LgBiT added. **C.** *IRSp53 enhances Arc release in HEK293T cells.* HEK cells were transfected with Arc alone or Arc+IRSp53 and Arc was detected by luciferase. Percentage Arc release was calculated by dividing the total Arc levels in the media by the sum of total Arc in the cell lysate and total Arc in the media (n=3 cultures). Statistics: ****p<0.0001, one-way ANOVA. Results are representative of experiments conducted in three different cultures. **D.** *HiBiT assay measures Arc EV release*. Arc release in HEK cells was almost undetectable in the absence of lysis, indicating that Arc-Hibit is protected within vesicles. **E.** *IRSp53 increases Arc particle size in EV fractions.* The size of Arc EVs was determined using nanoparticle tracking analysis (NTA). Particle tracks (n=3) are depicted as averages (blue and yellow line traces) with ± SEM depicted as shaded areas. **F.** *IRSp53 drives Arc release into EVs.* Equilibrium density gradient isolation was used to isolate Arc EVs from HEK cell culture media. The density in fractions 15-17 was between 1.10 and 1.15 grams/mL, consistent with the known densities of EVs. **G.** *IRSp53 enhances Arc release in neurons.* IRSp53-dependent enhancement of Arc release requires the interaction with actin machinery ($IRSp53^{I403P}$) and direct protein interaction with Arc ($Arc^{\Delta 20\text{-}40}$) (n=3 cultures). Statistics: **p<0.01, one-way ANOVA. **H.** *IRSp53 knockdown reduces Arc release.* Representative western blot of protein expression in EVs released from primary cortical neurons and blotted for Alix or Arc. Pooled quantification of EVs harvested from three independent cultures (n=3) for Arc and Alix, paired t-test comparing control and Cre expressing conditions. Arc EV expression was normalized to Alix. Statistics: *p<0.05, paired t-test.

We next tested whether IRSp53 enhanced Arc-HiBiT release in primary cultured hippocampal neurons. Neurons were transduced at DIV10 with Arc-HiBiT alone or with Arc-HiBiT+IRSp53. We find that IRSp53 enhances Arc release by approximately 2.5-fold in neurons (Figure 2G). Similar to HEK cells, $IRSp53^{I403P}$ does not enhance Arc-HiBiT release (Figure 2G). $Arc^{\Delta 20\text{-}40}$, which is unable to bind IRSp53, also does not enhance release when co-transduced with IRSp53 (Figure 2G). These data suggest that IRSp53 specifically enhances Arc release into EVs from neurons, through downstream actin regulation, and this effect requires direct protein-protein interactions with Arc.

To determine whether IRSp53 plays a role in the release of endogenous Arc in EVs from neurons, we obtained an IRSp53 floxed mouse line[28] and generated $IRSp53^{flx/flx}$ primary cultured neurons. Lentiviral expression of GFP-Cre for six days (DIV10-16) resulted in a significant reduction in IRSp53 expression in cell lysates (~60%) as compared with GFP expression, but no change in Arc or Alix (a canonical EV marker) expression (Supplemental Figure 2H). EVs were isolated from cell culture media using differential centrifugation on a sucrose cushion. Knockdown of IRSp53 significantly reduced the release of Arc into EVs (Figure 2H) but had no effect on Alix release (Figure 2H). Together, these results show that IRSp53 is critical for Arc EV biogenesis by facilitating both Arc capsid assembly and Arc EV release.

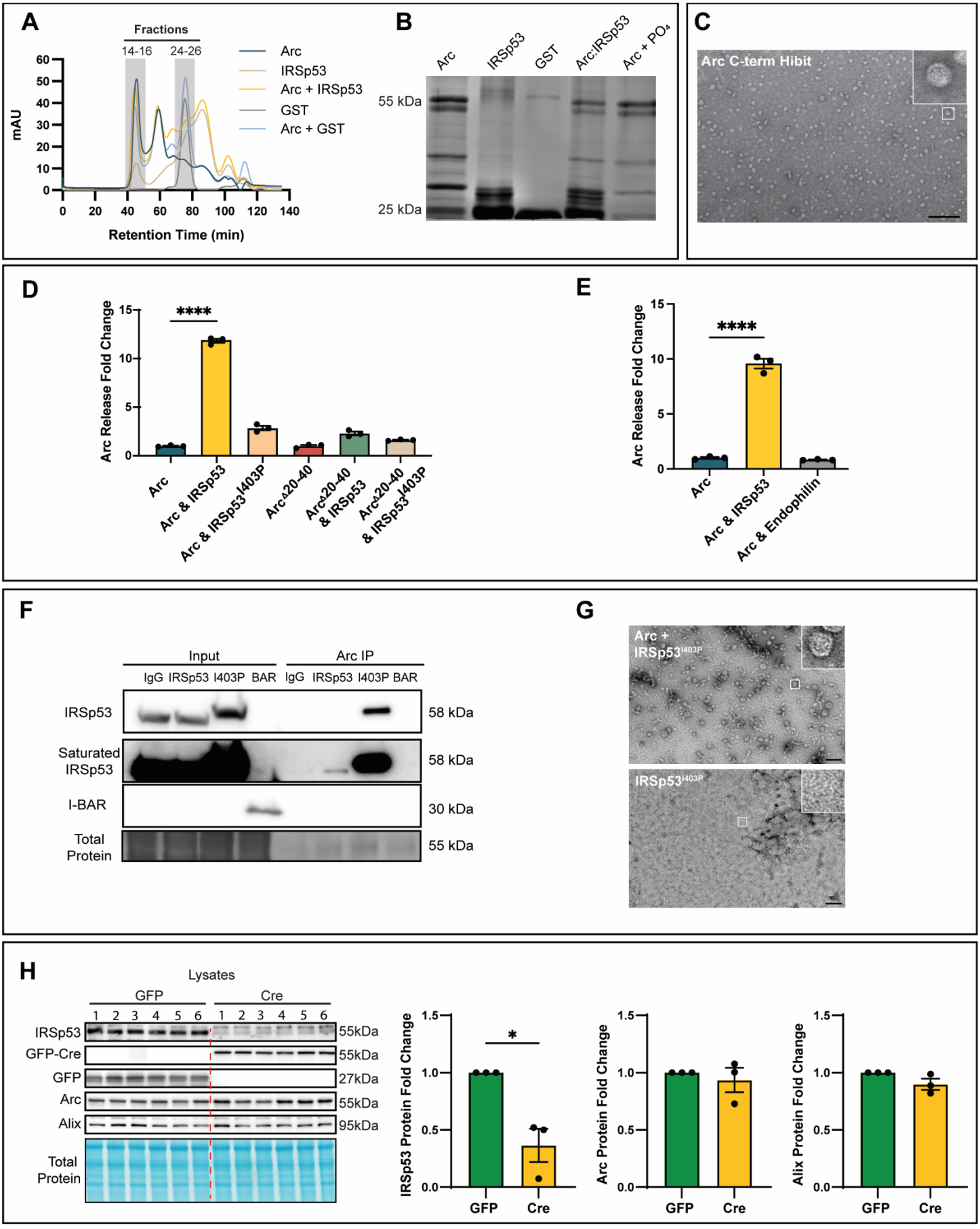

Supplementary Figure 2. IRSp53 facilitates Arc capsid assembly and release, related to Figure 2. A. Chromatogram showing SEC peaks selected for TEM. **B.** Coomassie gel showing protein content from the selected peaks. Arc, IRSp53, Arc + IRSp53, Arc + GST, and Arc +PO_4 were selected from fractions 14-16**,** while GST was selected from fractions 24-26. **C.** *Arc tagged with HiBiT at the C-terminal does not interfere with capsid formation.* Scale bar=200 nm. **D.** *IRSp53 enhanced Arc release is specific and requires its SH3 domain. IRSp53 does not enhance the release of* $Arc^{\Delta 20\text{-}40}$ (n=3 independent cultures). Statistics: ****p<0.0001, one-way ANOVA. **E.** *Endophilin, an N-BAR containing protein that also interacts with Arc, does not affect Arc release* (n=3 independent cultures). Statistics: ****p<0.0001, one-way ANOVA. **F.** $IRSp53^{I403P}$ *co-IPs with Arc.* HEK293 cells were transfected with Arc and IRSp53, $IRSp53^{I403P}$, and the IRSp53 I-BAR domain. Arc binds to both IRSp53 and $IRSp53^{I403P}$, but IRSp53's I-BAR domain does not. *Saturated*: Same western blot depicted in (**F**) for Arc co-IP samples with an increase in contrast to show IRSp53 does IP with Arc. **G.** $IRSp53^{I403P}$ *drives Arc capsid assembly similar to WT IRSp53.* **H.** *Cre expression in* $IRSp53^{flx/flx}$ *neurons reduces IRSp53 expression.* Representative primary cortical neuronal cell lysates run by SDS-Page, blotted for Alix, Arc, IRSp53, and GFP with total protein shown. Data is presented as mean±SEM from 3 independent cultures, normalized to total protein and average of control conditions to determine relative fold change is shown. Paired student t-test performed comparing control and Cre expressing conditions. Statistics: *p<0.05, paired t-test.

LTP induces the expression, trafficking, and release of Arc via IRSp53.

Arc and IRSp53 expression in neurons is regulated by neuronal activity[12,23]. Although Arc is not required for the maintenance of LTP[13], Arc transcription is induced by LTP stimuli[12]. Thus, we hypothesized that LTP induces Arc capsid assembly and release through IRSp53-dependent mechanisms. We quantified endogenous Arc and IRSp53 expression in cultured hippocampal neurons under basal conditions or after chemical induction of LTP or LTD (cLTP/cLTD). To induce cLTP, neurons were incubated with TTX for 24 hours to block neuronal activity, followed by a 5-minute glycine pulse and recovery in normal culture media. To induce cLTD, a 5-minute DHPG pulse was performed in normal culture media. To verify whether cLTP or cLTD occurred, we labeled surface GluA1 AMPAR subunits in living neurons and found that cLTP results in an increase in surface GluA1 staining, while cLTD leads to a reduction in surface GluA1 expression (Figure 3A-B, Supplementary Figure 3A-B). Arc expression increases in dendrites after both cLTP and cLTD, with no changes observed in the soma (Figure 3C, Supplementary Figure 3A, C). We also observed a selective increase in IRSp53 expression in dendrites but not the soma after cLTP, but not cLTD (Figure 3D; Supplementary Figure 3A, D). Using Imaris software, we analyzed the percentage of IRSp53 that was Arc positive (colocalized) or Arc negative (not colocalized). Both cLTP and cLTD increased the number of Arc "surfaces" (expression), but only cLTP increased IRSp53-Arc colocalization (Figure 3E-F). These data suggest that LTP induces the expression of both Arc and IRSp53 in dendrites to facilitate their interaction.

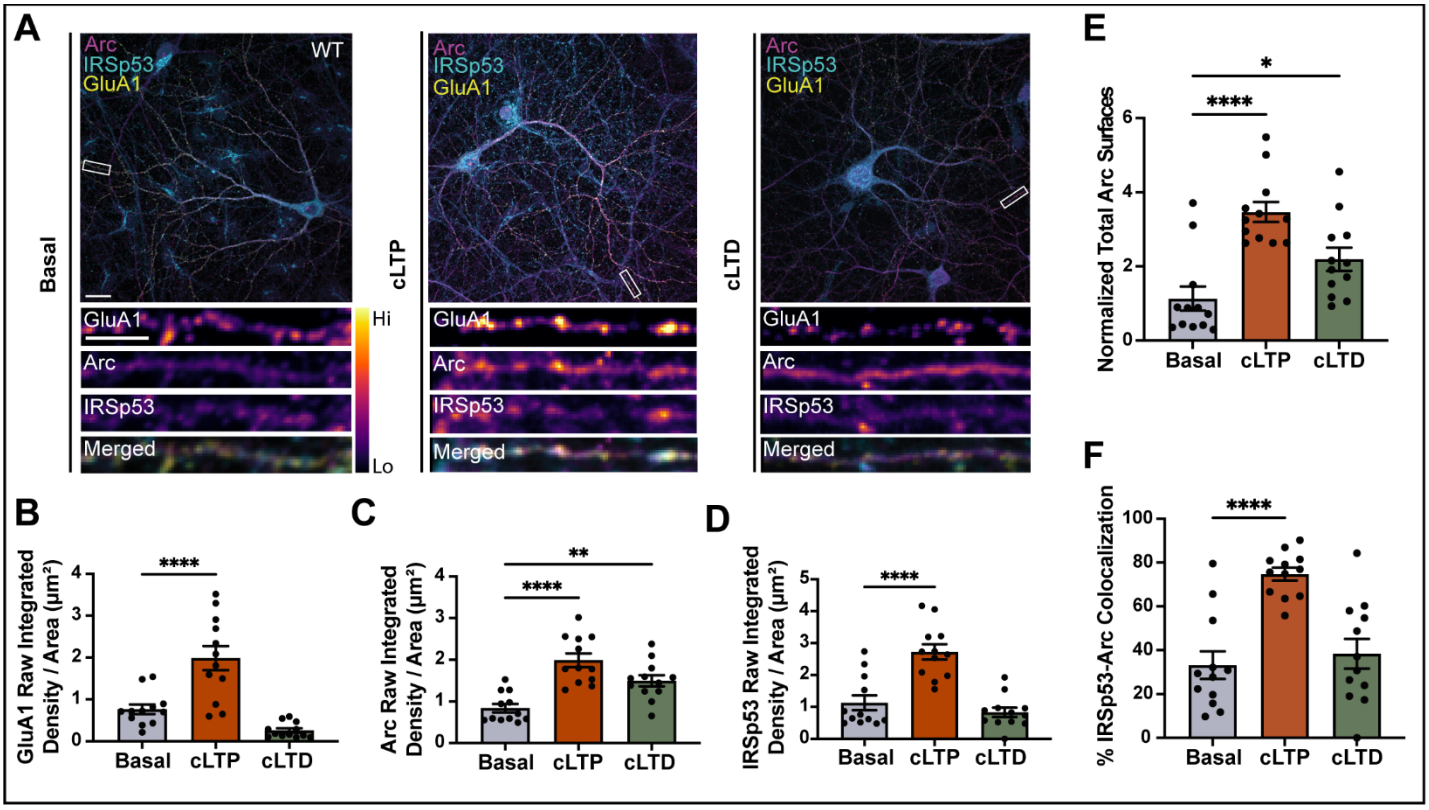

Figure 3. LTP induces Arc and IRSp53 colocalization in neurons. A. Representative images of primary cultured rat hippocampal neurons (DIV16) under basal, cLTP or cLTD conditions. Scale bar=20µm. Dendritic scale bar=5µm. 30 min. post cLTP/cLTD surface GluA1 was labeled with an N-terminal antibody and neurons were fixed/stained for Arc (magenta), IRSp53 (cyan), and GluA1 (yellow). **B-D.** *cLTP and cLTD induces Arc expression in dendrites, but only cLTP induces an increase in IRsp53 expression.* Quantification of dendritic Arc, IRSp53, and surface GluA1. Three 2µm dendritic segments were measured per neuron (n=14 neurons from 3 coverslips). Statistics: GluA1 ****p<0.0001, Arc **p<0.01, ****p<0.0001, IRSp53 ****p<0.0001, one-way ANOVA. **E.** *cLTP and cLTD increases Arc expression in dendrites*. An algorithm was generated using the surface function in Imaris software to detect the total Arc volume in each image and the same algorithm was applied to all images. Statistics: *p<0.05, ****p<0.0001, one-way ANOVA. **F.** *Arc and IRSp53 colocalization increases during cLTP but not cLTD.* Quantification of Arc volumes detected in each image using the Imaris surface function. Statistics: ****p<0.0001, one-way ANOVA. Results are representative of experiments conducted in two different cultures.

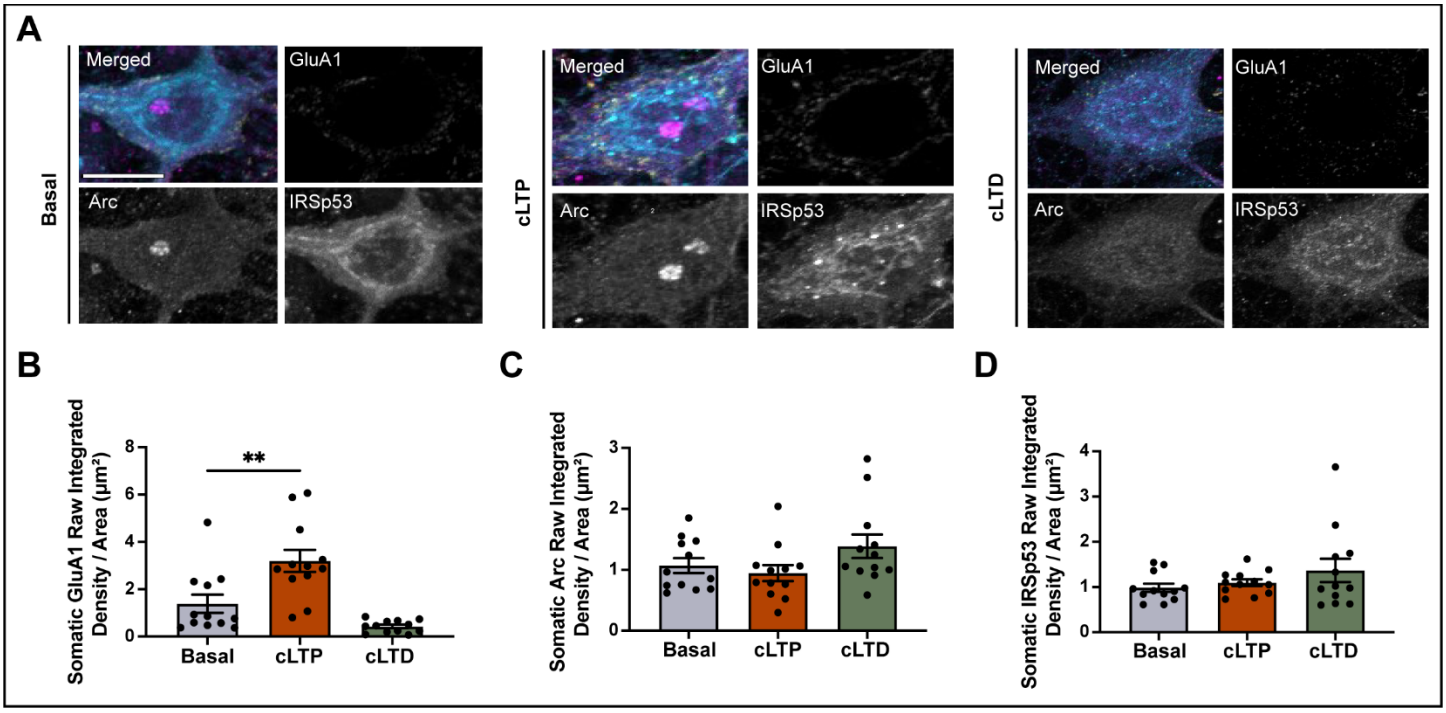

Supplementary Figure 3. Neither cLTP or cLTD affect expression of Arc or IRSp53 in neuronal soma, related to Figure 3. A. Representative images of primary cultured rat hippocampal neurons (DIV16) under basal, cLTP or cLTD conditions (n=14 neurons from 3 coverslips). Scale bar=10µm. Arc (magenta), IRSp53 (cyan), and GluA1 (yellow). **B-C.** *cLTP increases somatic surface GluA1 staining, but not Arc or IRSp53 expression.* Quantification of somatic Arc, IRSp53, and surface GluA1. **D.** *cLTD does not increases GluA1, Arc or IRSp53 expression*. *Statistics: GluA1 **p<0.01, one-way ANOVA.* Results are representative of experiments conducted in two different cultures.

To probe the dynamics of Arc and IRSp53 in living cells, we developed Arc-RaPTR (RNA and Protein Translation Reporter) that allows imaging of Arc protein and mRNA (Figure 4A). The Arc N-terminus includes hemagglutinin (HA) epitopes that allow protein tagging, while the C-terminus includes a number of MS2 tandem repeats that allow labeling of mRNA. Exogenously added α-HA-FB-eGFP Frankenbodies and MS2 coat protein labelled with miRFP703 allows imaging of nascent protein or mRNA, respectively[29]. Expression of this construct was driven by the ESARE Arc minimal promoter, which recapitulates the activity-dependent regulation of Arc transcription[30]. DIV14 hippocampal neurons were transfected with Arc-RaPTR alone or co-transfected with a C-terminal mRuby labeled IRSp53 (Figure 4A). Neurons were imaged for 15 minutes during TTX treatment and for 1-2 hours following cLTP induction in cell culture media. cLTP induction increased Arc-RaPTR expression (Figure 4B, Supplementary 4A) and increased the anterograde trafficking of *Arc* mRNA and protein in dendrites (Supplementary Movie 1). In IRSp53 co-transfected neurons, Arc and IRSp53 puncta colocalized and trafficked together in dendrites after cLTP induction (Figure 4C, Supplemental Figure 4B), although there was no significant difference in the total number of trafficking events as compared to Arc transfection alone (Supplementary Figure 4C). After cLTP induction, we occasionally observed transient formation of filopodial-like protrusions in dendrites containing Arc and IRSp53 (Figure 4D and Supplementary Movie 2). These projections were accompanied by rapid loss of Arc signal, which we interpret as possible release events.

To directly determine whether LTP induces Arc release, neurons were transduced at DIV10 with Arc-HiBiT lentivirus and we quantified Arc-HiBiT release after cLTP or cLTD induction at DIV16 (Figure 4E). We found that cLTP robustly induced Arc-HiBiT release, compared with basal and cLTD conditions (Figure 4F). To determine whether cLTP-induced Arc release is IRSp53-dependent, we used primary cortical IRSp53$^{flx/flx}$ neurons that were co-transduced with either GFP+Arc-HiBiT or Cre+Arc-HiBiT lentiviruses. We observed a significant reduction in dendritic IRSp53 expression in IRSp53$^{flx/flx}$ neurons transduced with Cre, but no change in Arc expression (Supplementary Figure 4D-F). cLTP increased dendritic IRSp53 and Arc expression (Supplementary Figure 4 E-F) and enhanced Arc release in GFP transduced IRSp53$^{flx/flx}$ neurons (Figure 4G). In contrast, there was no significant change in Arc release after cLTP in IRSp53$^{flx/flx}$ neurons transduced with Cre (Figure 4G), suggesting IRSp53 is required for cLTP-induced Arc release. Interestingly, cLTP did not increase dendritic Arc expression in IRSp53$^{flx/flx}$ neurons transduced with Cre (Supplementary Figure 4F), suggesting that IRSp53 could be involved in Arc trafficking or expression in dendrites. These data show that cLTP induces Arc and IRSp53 colocalization, anterograde trafficking and release from dendrites.

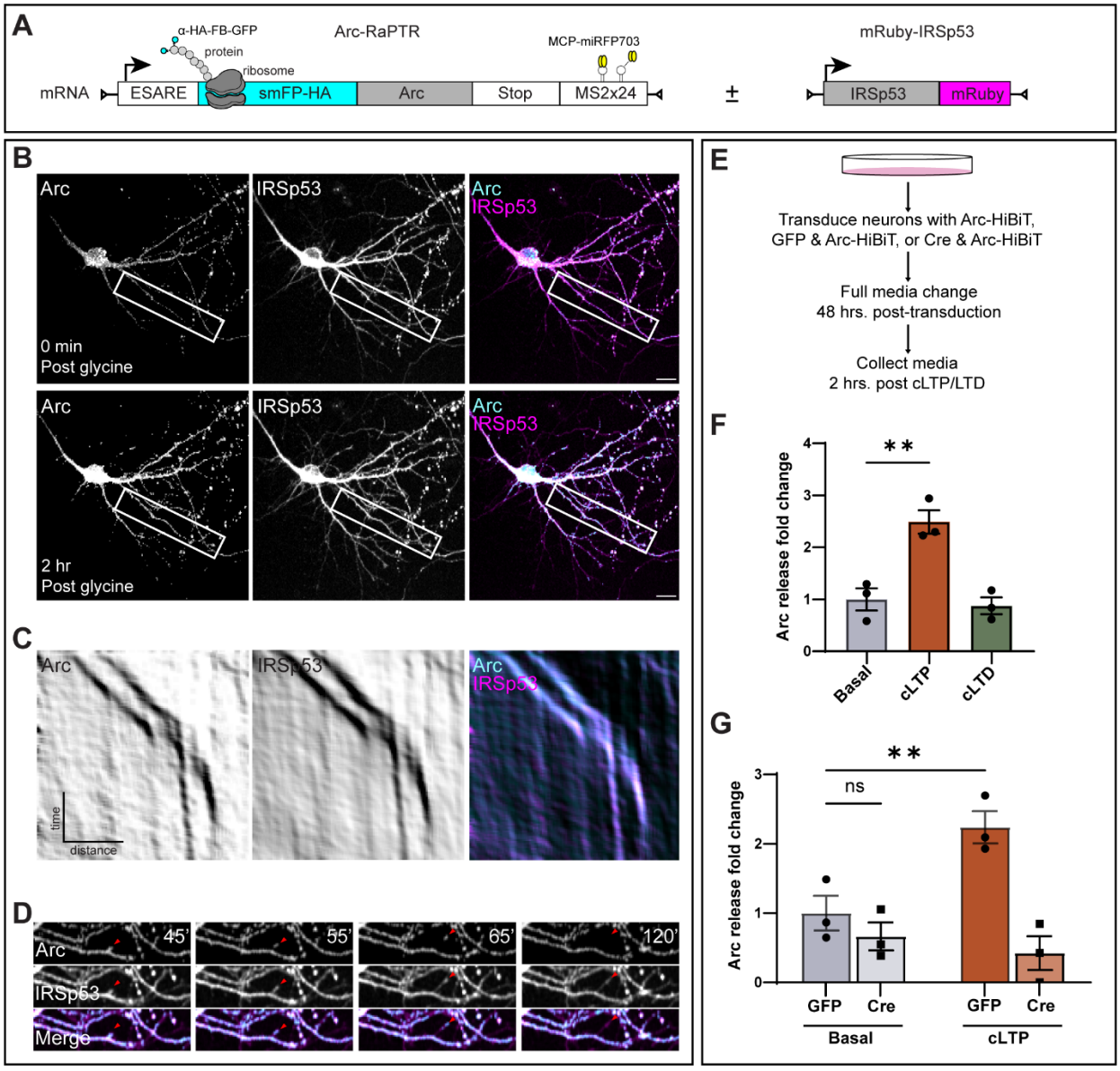

Figure 4. LTP induces Arc trafficking and release via IRSp53 filopodia. A. *Arc RNA and Protein Translation Reporter (RaPTR).* The *Arc* mRNA contains spaghetti-monster Frankenbody hemagglutinin epitopes at the 5' end and 24 MS2 RNA stem-loops at the 3' end. α-HA-FB-eGFP Frankenbodies bind to translated protein, while (MCP)-miRFP703 binds to *Arc* mRNA allowing for dual labeling of Arc protein and mRNA. **B.** *cLTP induces Arc-RaPTR expression.* Representative max projection images of neurons co-transfected with the Arc-RaPTR reporter and a C-terminally tagged mRuby-IRSp53 immediately or 2 hours after cLTP induction. **C.** *LTP induces anterograde co-trafficking of Arc and IRSp53 in dendrites.* Representative forward filtered kymograph of a dendritic region of interest (ROI) from a dendrite in panel B. Time is displayed on the y-axis (bar=25 min.) and distance on the x-axis (bar=30 μm). **D.** *Putative Arc release events occur from newly formed filopodial-like projections.* Dendritic ROI showing an IRSp53 labeled filopodia with Arc at the leading tip (red arrows). There is a rapid loss of Arc signal from this extension. **E.** Schematic for neuronal transduction protocol for the HiBiT assay. **F.** *LTP induces Arc release.* cLTP, but not cLTD, increases HiBiT-Arc release. Statistics: **p<0.01, one-way ANOVA. Each data point represents one well from a 6-well plate (technical replicates). Results are representative of experiments conducted in 3 different cultures. **G.** *IRSp53 is necessary for cLTP induced Arc-HiBiT release. IRSp53$^{flx/flx}$* neurons were transduced at DIV10 with GFP or GFP-Cre to knockdown IRSp53 expression. Statistics: **p<0.01, two-way ANOVA, Tukey's multiple comparison test. Each data point represents one well from a 6-well plate (technical replicates). Results are representative of experiments conducted in two different cultures.

Arc EVs induce loss of surface AMPARs in recipient neurons via translation of *Arc* mRNA.

Since cLTP induces Arc EV release, we set out to investigate whether Arc EVs can directly regulate synaptic plasticity by trafficking the AMPA-type glutamate receptors in neurons that take up Arc EVs. We collected media from DIV15 WT or Arc KO mouse cortical neurons and isolated EVs using SEC. 50μg of EVs in fresh BrainPhys neuronal media were added to DIV 15 mouse Arc KO neurons for 4 hours, followed by a live antibody feeding assay to label surface GluA1[11]. Neurons treated with WT EVs showed a significant reduction in surface GluA1 levels, whereas neurons treated with Arc KO EVs showed no difference in surface GluA1 (Figure 5A). These effects on GluA1 may be mediated by Arc protein or *Arc* mRNA delivered in EVs. To test this, we transduced Arc KO recipient neurons with an Arc-specific shRNA lentivirus, which blocks the translation of *Arc* mRNA (Supplemental Figure 5). Neurons transduced with Arc-shRNAs showed no changes in surface GluA1 when incubated with WT EVs, while neurons transduced with scrambled shRNAs showed decreased surface GluA1 levels after WT EV incubation (Figure 5B). These data suggest that Arc EVs induce the loss of surface GluA1 in recipient neurons via the translation of delivered *Arc* mRNA.

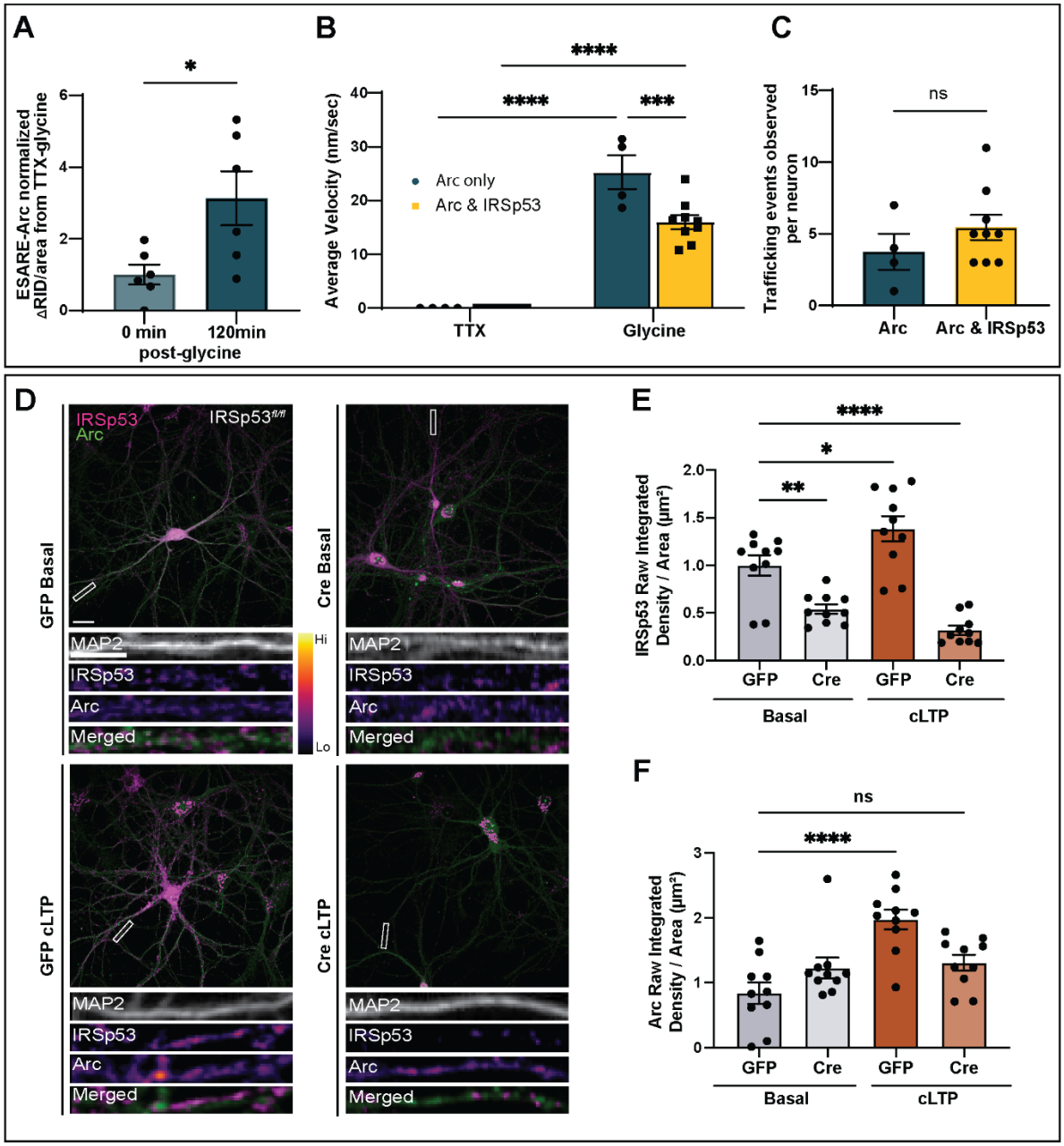

Supplementary Figure 4. LTP induces trafficking of Arc and IRSp53 in dendrites, related to Figure 4. A. *LTP induces Arc-RaPTR expression.* cLTP induction increased the expression of Arc-RaPTR in co-transfected neurons (n=6 neurons). Statistics: *p<0.05, outliers were excluded using the ROUT method, Q=1%. **B.** The average velocity of Arc (25.27 nm/sec), and co-localized Arc and IRSp53 (16.011 nm/sec) puncta during anterograde trafficking induced by cLTP (n=4 neurons for Arc only, n=9 neurons for Arc & IRSp53). Statistics: ***p<0.0007, **** p<0.0001. **C.** *IRSp53 overexpression does not affect Arc particle velocity.* There is no difference in particle velocity between single and co-transfected neurons (n=4 neurons for Arc only, n=9 neurons for Arc & IRSp53). **D.** Representative images of IRSp53$^{flx/flx}$ primary cultured mouse hippocampal neurons under basal or cLTP conditions. Scale bar=20µm. Dendritic scale=5µm. Neurons were transduced with GFP or GFP-Cre lentiviral particles at DIV10 and neurons were fixed DIV16. **E.** *IRSp53 knockdown inhibits cLTP induced IRSp53 expression*. Quantification of dendritic IRSp53. Three 20µm dendritic segments were measured per neuron (n=10 neurons from 3 coverslips). Statistics: *p<0.05, **p<0.01, ****p<0.0001, one-way ANOVA. **F.** *IRSp53 knockdown inhibits cLTP induced dendritic Arc expression*. Quantification of dendritic Arc. Three 20µm dendritic segments were measured per neuron (n=10 neurons from 3 coverslips). Statistics: ****p<0.0001, one-way ANOVA. Results are representative of experiments conducted in two different cultures.

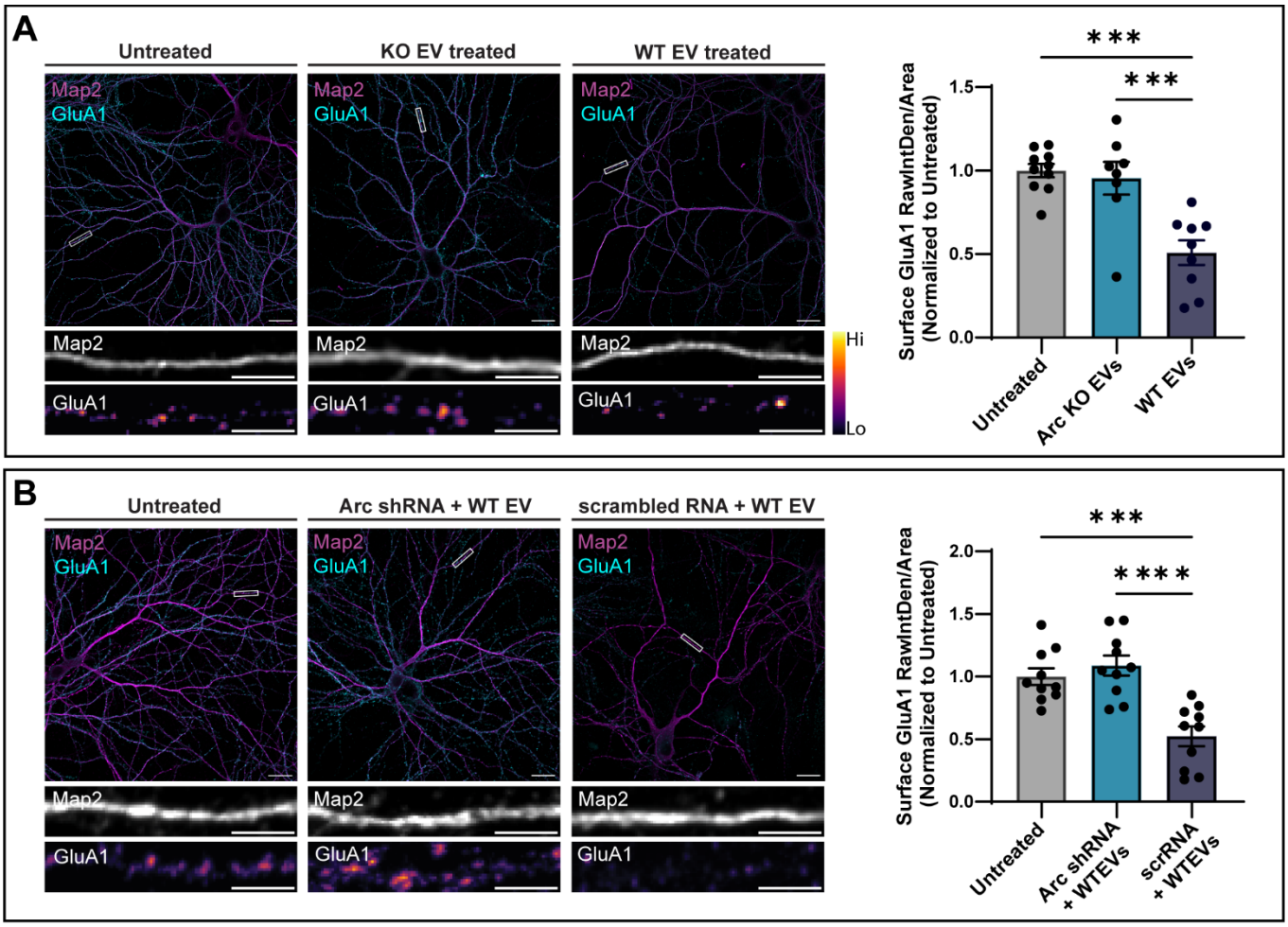

Figure 5. Arc EVs decrease surface GluA1 expression in recipient neurons via *Arc* mRNA translation. A. *Arc containing EVs induce loss of surface GluA1.* Representative images of neurons that were untreated, or treated with EVs derived from WT neurons, or with EVs from Arc KO neurons. Scale bar=20μm. Dendritic scale=5μm. Three 20μm dendritic segments were measured per neuron (n=8-10 neurons from 3 coverslips). Results are representative of experiments conducted in at least two different cultures. Statistics: ***p<0.0001, one-way ANOVA. **B.** *Translation of Arc mRNA is required for effects on surface GluA1.* Representative images of neurons that were untreated or transduced with either Arc shRNA or scrambled shRNAs at DIV 10 and treated with WT EVs on DIV 15. Three 20μm dendritic segments were measured per neuron (n=12 neurons from 3 coverslips). Results are representative of experiments conducted from two different cultures. Statistics: ***p<0.0005, ****p<0.0001, one-way ANOVA.

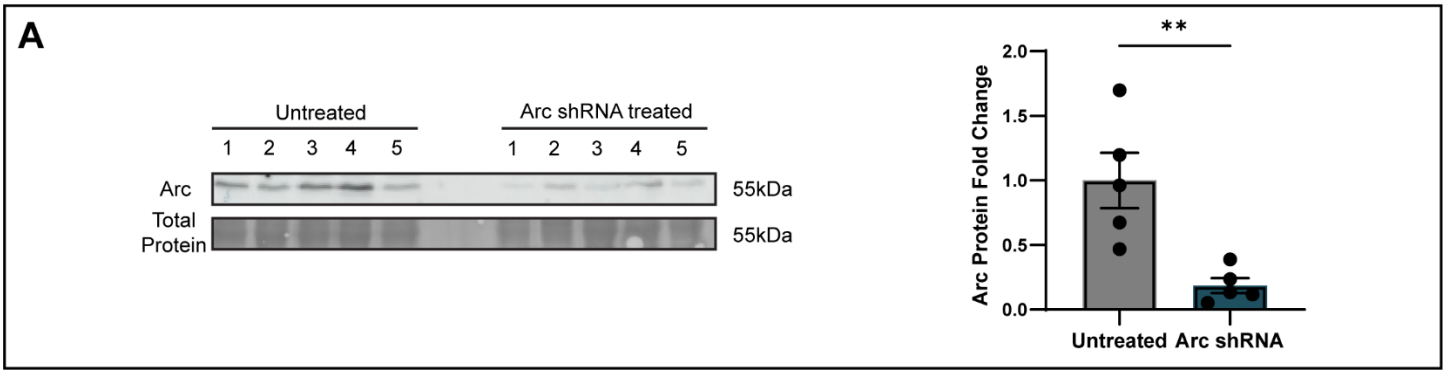

Supplemental Figure 5. Arc shRNA reduces Arc expression in neurons, related to Figure 5. A. WT cortical neurons were transduced with Arc-shRNAs or left untreated. Arc shRNAs significantly reduce the amount of Arc expressed in WT neurons. Densitometric analysis was performed in FIJI (n=5 10cm dishes from one culture). Statistics: **p<0.007, unpaired t-test.

Arc protein transfer causes a loss of surface AMPARs in neighboring neurons.

To determine whether Arc transfer between neurons regulates AMPAR expression, we sparsely transfected primary mouse hippocampal Arc KO neurons with either GFP alone or GFP+Arc (Figure 6A-B) and analyzed Arc expression in neighboring neurons and dendrites (Supplementary Figure 6). We observed a significant increase in dendritic Arc staining in neurons neighboring Arc-transfected neurons, as compared to neighbors of GFP-transfected neurons, but no change in somatic staining (Figure 6C-D). Mouse neurons were difficult to transfect and live label with GluA1 due to health issues, while rat hippocampal neurons survived transfection and live surface GluA1 labeling. We generated an Arc KO rat using CRISPR (Supplementary Figure 7). In rat Arc KO neurons sparsely transfected with GFP or GFP+Arc, we observed a significant decrease in surface GluA1 in dendrites of Arc transfected neurons but not in GFP only transfected neurons (Figure 6E-G). We also observed a significant decrease in surface GluA1 staining in neighboring dendrites spatially proximal to Arc transfected neurons, but no change in neighboring dendrites near GFP transfected neurons (Figure 6H-J). However, we did not observe changes in GluA1 surface expression in neurons more than 450μm from Arc transfected donor neurons in the same coverslip (Figure 6G-H, J). Together, these data suggest that Arc protein is transferred to spatially proximal neighboring dendrites that take up Arc, which causes a loss of surface GluA1.

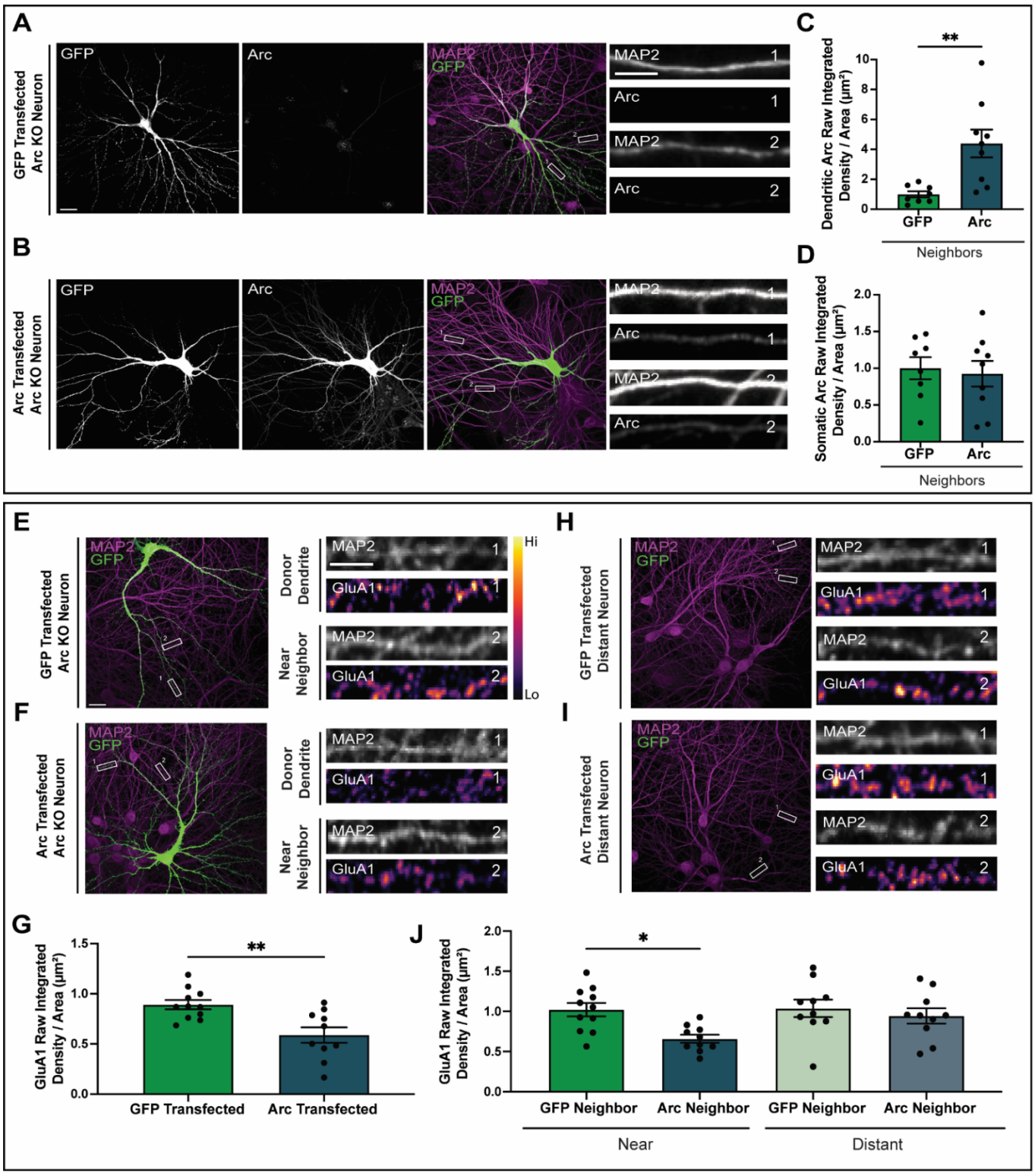

Figure 6. Intercellular Arc transfer induces loss of surface GluA1 in neighboring dendrites. A. Representative image of a GFP transfected primary cultured mouse Arc KO hippocampal neurons that were stained for Arc and MAP2 at DIV15. Scale bar=20µm. Dendritic scale=5µm. See Supplementary Figure 6 for analysis details. **B.** Representative image of an Arc and GFP co-transfected mouse Arc KO hippocampal neuron. **C.** *Arc is transferred from transfected neurons to neighboring dendrites.* Quantification of dendritic Arc raw integrated density for dendrites located near GFP alone or Arc+GFP transfected neurons (n=8-12 neurons from 3 coverslips). Statistics: **p<0.01, unpaired t-test. Results are representative of experiments conducted in two different cultures. **D.** *Arc does not transfer from transfected neurons to nearby neuronal somas.* Quantification of Arc raw integrated density for neuronal somas near GFP or Arc transfected

neurons. (n=8-12 neurons from 3 coverslips). **E.** Representative image of a GFP transfected rat primary cultured Arc KO hippocampal neuron that was stained for MAP2 and surface GluA1 at DIV15. Dendritic scale bar=5μm. **F.** Representative image of an Arc and GFP co-transfected rat Arc KO hippocampal neuron. **G.** *Surface GluA1 is significantly reduced in Arc+GFP co-transfected neurons compared to GFP transfected alone*. Quantification of surface GluA1 raw integrated density (n=10-12 neurons from 3 coverslips). Statistics: **p<0.01, unpaired t-test. Results are representative of experiments conducted in three different cultures. **H.** Representative image of a neuron that does not have a GFP transfected neuron in the field of view. **I.** Representative image of a neuron that does not have an Arc+GFP transfected neuron in the field of view. **J.** *Surface GluA1 is significantly decreased in dendrites near Arc transfected neurons, but not in distant dendrites*. All surface GluA1 levels in dendrites were normalized to the dendrites near GFP transfected neurons (n=10-12 neurons from 3 coverslips). Statistics: *p<0.05, one-way ANOVA. Results are representative of experiments conducted in three different cultures.

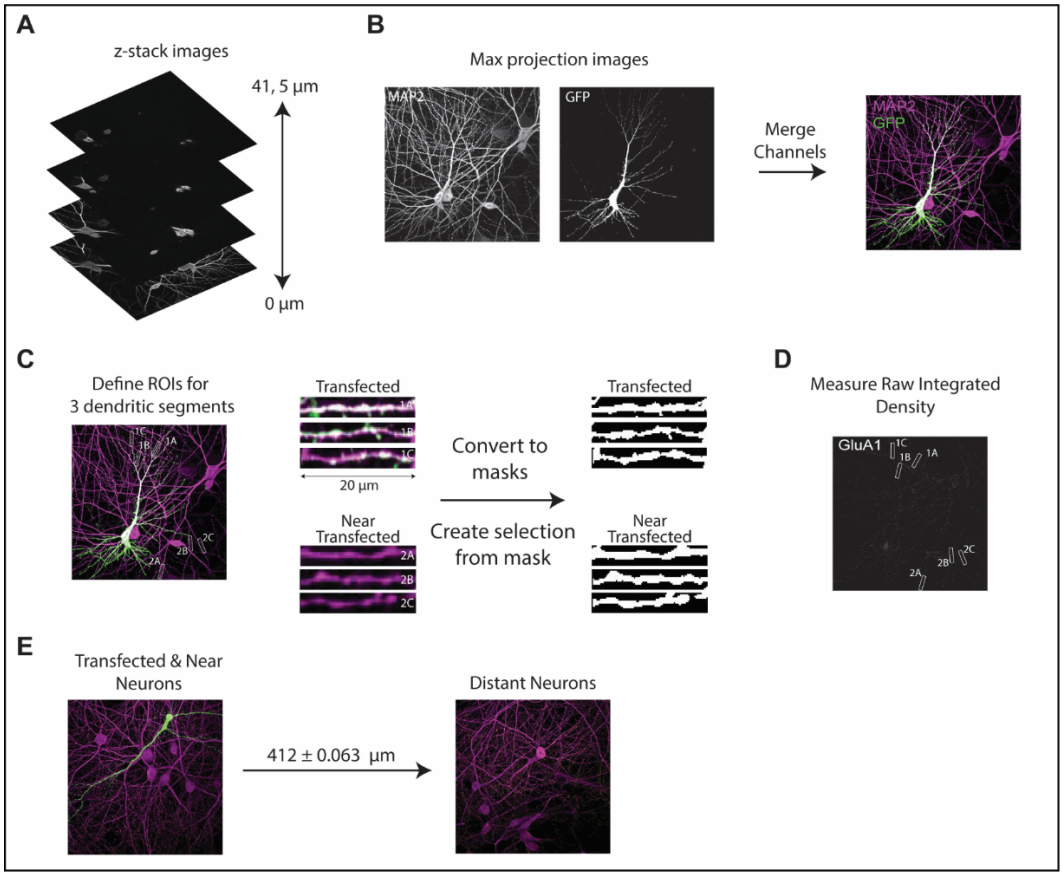

Supplementary Figure 6. GluA1 analysis pipeline, related to Figure 6. A. *GluA1 analysis pipeline*. Z-stack images were acquired using 0.125 μm step size resulting in 41 images. **B.** Max projection images were created from the z-stack for the MAP2 channel and GluA1 and the channels were merged. Untransfected neurons underwent thresholding in FIJI to find an average threshold value. This value was then applied to all images. **C.** ROIs were defined for three GFP positive dendritic segments and three GFP (untransfected) negative dendritic segments near a GFP transfected neuron by MAP2 staining. The segments were then converted to masks. **D.** These masks were applied to the GluA1 channel and raw integrated density was measured for all dendritic ROIs. The three dendritic segments were averaged together to obtain a single value for each neuron. All dendritic segments were normalized to untransfected near neighbors of GFP transfected neurons. **E.** Distant neurons were defined by centering a GFP transfected neuron and move the frame until all of the GFP transfected neuron was out of frame. This averaged ~400μm from a transfected neuron.

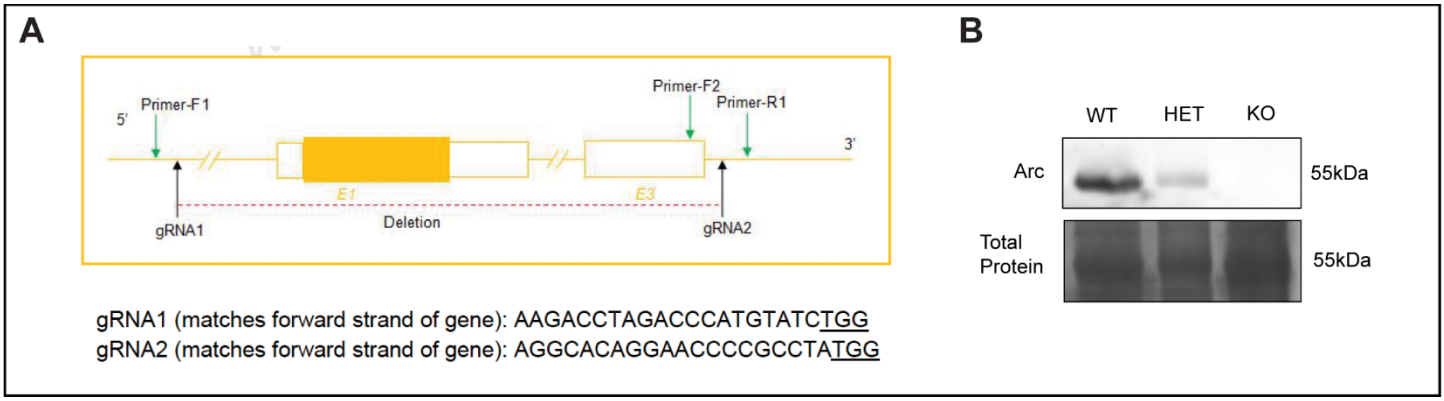

Supplementary Figure 7. Arc KO rat characterization, related to Figure 6. A. Schematic depicting the CRISPR design strategy for excising the entire *Arc* gene in Long Evan rats. Embryos were injected with gRNAs and dCAS9 before being implanted in a dam. Deletion of the *Arc* gene was detected by PCR, using primers against the *Arc* gene. **B.** *Arc protein is absent in Arc KO rat brain tissue.* Western blot of rat forebrain tissue collected from WT, heterozygous, or Arc KO rats.

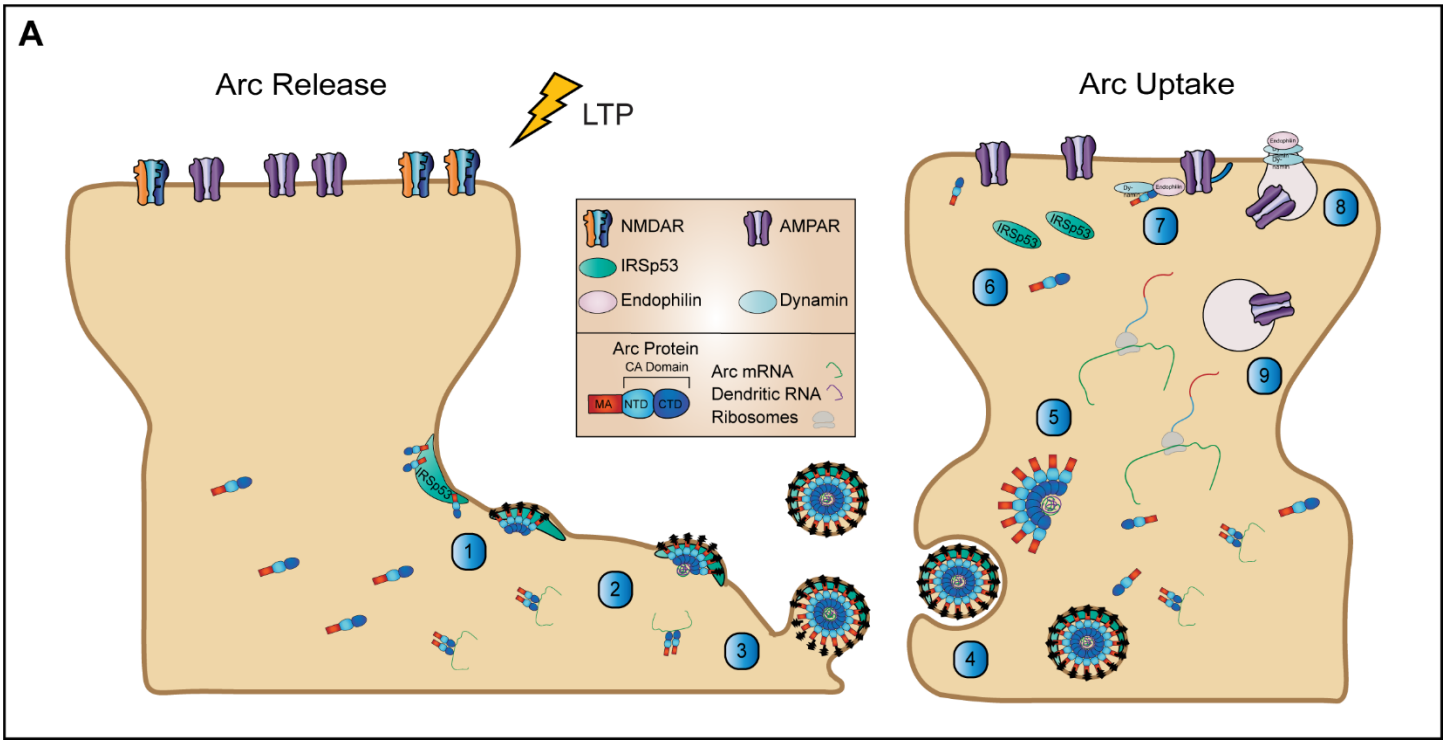

Supplementary Figure 8. Model of Arc intercellular synaptic plasticity. A. LTP induces: **1.** Arc and IRSp53 expression in dendrites. **2.** IRSp53 facilitates Arc oligomerization into capsids through N-terminal interactions, which assemble at the membrane and encapsulate *Arc* mRNA. **3.** Arc capsids are released in EVs directly from filopodia-like projections at the plasma membrane. **4**. Neighboring dendrites take up Arc EVs via endocytosis. **5.** *Arc* mRNA is released from endosomes as the capsid is disassembled and is locally translated in dendrites. **6.** Nascent Arc protein monomers are recruited to the synapse. **7.** Arc interacts with the endocytic machinery (dynamin and endophilin) to **8.** recruit and endocytose AMPARs from the synapse. **9.** Arc traffics the AMPARs out of the synapse.

Discussion

The unexpected discovery that Arc forms virus-like capsids that are released from neurons[6] implied that there must be an Arc-dependent intercellular function in the brain. Here, we show that Arc mediates a novel form of intercellular synaptic plasticity (Supplementary Figure 8). LTP induces the release of Arc EVs from dendrites, which deliver *Arc* mRNA to nearby dendrites. The delivered *Arc* mRNA is translated, which ultimately results in a loss of surface AMPARs to weaken synapse strength. We also reveal a central role for IRSp53 in regulating Arc capsid assembly and release into EVs – identifying a new mechanism for neuronal EV biogenesis.

IRSp53 facilitates Arc capsid assembly

Retroviruses use scaffolding molecules, such as inositol hexakisphosphate (IP_6) or nucleocapsid proteins, to provide structural support during capsid assembly[31,32]. Mammalian Arc has structural homology to HIV capsids, and *Drosophila* Arc proteins assemble retrovirus-like icosahedral capsids[33]. Here, we find that IRSp53 protein can directly facilitate the assembly of Arc capsids *in vitro*. Whether IRSp53 plays a similar function in retrovirus capsid assembly remains to be determined. Our data also shows that the role of IRSp53 in EV release can be dissociated from its role in Arc capsid assembly as the IRSp53^{I403P} mutant does not enhance Arc release, presumably due to a lack of downstream actin regulation through SH3 domain interactions[27], but can still facilitate Arc capsid assembly.

IRSp53 is required for Arc EV release

EV intercellular signaling has emerged as a critical component of diverse biological processes, from plant defenses against microbes[34] to the spread of pathology in neurodegenerative disorders[35]. However, the function of neuronal EVs remains poorly described, and their role in the nervous system is unclear[36]. This is partly due to a need for a mechanistic understanding of the biogenesis and cargo of select EVs. EVs have a variety of intracellular origins, with exosomes derived from endosomal compartments that are released via multivesicular bodies requiring ESCRT protein complexes for vesicle biogenesis[14]. Recent studies have shown that EVs may participate in synaptic function through intercellular transfer of synaptobrevin[37] and regulation of Wnt signaling through the protein proline-rich 7[38]. Previous studies showed that AMPARs may be released in EVs[15]. Neuron-derived exosomes may also be critical for neural circuit development[39]. In addition, intercellular trafficking of toxic proteins in EVs such as tau and α-synuclein have been implicated in the pathology of Alzheimer's and Parkinson's disease[35].

IRSp53 is an I-BAR scaffolding protein highly expressed in neurons that regulates dendritic spine formation and NMDA receptor function[40-42]. Recent studies have implicated IRSp53 in EV release in non-neuronal cells via direct budding from the plasma membrane[17,18,22]. Our data reveals a neuronal activity-dependent EV pathway regulated by IRSp53. We find that IRSp53 expression is upregulated in dendrites after LTP induction, which we hypothesize also increases Arc-IRSp53 interactions to catalyze capsid assembly. Arc-IRSp53 complexes traffic anterograde in dendrites where EV release occurs. This spatiotemporal protein trafficking may specify where and when Arc EVs are released. In our live imaging experiments, we observed the rapid formation of filopodia

that contain Arc and IRSp53 proteins, and, in some cases, there was an abrupt loss of Arc protein suggestive of a release event. This is consistent with non-neuronal cell studies showing that IRSp53 may help induce filopodia formation[22], ultimately leading to EV biogenesis similar to another I-BAR protein MIM[43,44].

Arc and LTP

Arc transcription is clearly induced by LTP stimuli[12,45]. However, there is conflicting evidence for the role of Arc in the expression of LTP. LTP is intact in the hippocampus of Arc KO mice, but Arc-specific antisense oligonucleotides cause deficits in dentate gyrus LTP[2,13,46,47]. Arc's role in LTD is clearer, with well-defined molecular mechanisms implicating Arc in the endocytosis of AMPARs[9,48-50]. Here, we resolve some of these discrepancies by showing that LTP, rather than LTD stimuli, preferentially causes the release of Arc. This switch in Arc function may be primarily mediated by an increase in dendritic expression of IRSp53, which catalyzes Arc capsid assembly. LTD stimuli, in contrast, induces local Arc translation that results in AMPAR endocytosis at synapses. We posit that synaptic Arc protein regulates AMPAR trafficking in a monomeric form, as post-synaptic density (PSD) protein-protein interactions may prevent Arc oligomerization[51].

Intercellular synaptic plasticity

Arc is critical for memory consolidation[2,47] and experience-dependent plasticity[52,53]. Recent studies have shown that Arc transcription can self-regulate cycles of transcription in a second wave of expression in the same neuron[54]. Thus, Arc synthesis may be sustained in neurons active during memory encoding. Our findings suggest that memory formation may involve intercellular signaling that requires non-cell autonomous regulation of synaptic function – a new element to mechanisms of memory formation. We predict that the spatial and temporal aspects of Arc release will be critical for regulating intercellular synaptic plasticity. These slow processes take hours from Arc transcription to Arc EV uptake, on par with the temporal evolution of the molecular consolidation of memory[55]. We observed a tight spatial constraint on Arc's effect on synapses, even in primary cultured neurons – only closely neighboring dendrites show AMPAR effects. We speculate that Arc facilitates a novel form of circuit-level LTD that may help consolidate memory by increasing the "signal-to-noise" of neurons in a memory "engram" circuit by weakening synapses neighboring non-engram neurons. This experience-dependent acceleration of synapse turn-over may also contribute to representational drift and memory updating[56]. This is similar to the hypothesis that Arc mediates heterosynaptic LTD on the same neuron[57], but now includes non-connected synapses near the active neuron in a circuit. Potentiated synapses on the neuron that transcribes Arc may be resistant to Arc-induced LTD from paracrine-like effects, perhaps through interactions with CaMKII-beta that localize Arc protein to inactive synapses[57].

Our new observations lead to a number of open questions. The dependency of *Arc* mRNA transfer for the functional effects on AMPARs suggests that once Arc EVs are taken up, *Arc* mRNA must be delivered and released into the cytoplasm, where it is translated. The precise molecular mechanisms of Arc capsid disassembly and mRNA release from endosomes remain to be elucidated. The specificity of Arc EV uptake *in vivo* also

remains to be determined; we hypothesize that unique receptors engage in Arc-EV uptake and delivery that will further constrain the spatial specificity of Arc EV function within a circuit.

Conclusion

Taken together, our data reveals a new EV-dependent intercellular signaling pathway regulated by IRSp53 and Arc. Arc EVs induce loss of surface AMPARs in recipient neurons to mediate an intercellular form of LTD. Our findings resolve previous studies showing that LTP induces Arc expression despite not playing a critical role in LTP itself. Our studies are the first to imply that intercellular synaptic plasticity may be important for memory consolidation. Future work will test these novel hypotheses and the precise function of Arc EVs *in vivo*. IRSp53 has been implicated in psychiatric disorders such as autism spectrum disorder (ASD), schizophrenia, and attention-deficit/hyperactivity disorder (ADHD)[40,58,59]. Future work will determine whether IRSp53-dependent EV biogenesis is disrupted in these disorders and whether IRSp53-Arc interactions can be targeted for potential therapeutic treatments.

Limitations

These studies were performed in primary cultured neurons, allowing molecular control over Arc expression, and distinguishing non-cell autonomous effects. However, we do not know whether LTP induces Arc release *in vivo* or if similar spatial signaling and intercellular synaptic plasticity occurs. Future studies will need to develop molecular tools to determine Arc donor and recipient cells in the intact brain, which will ultimately determine how Arc intercellular signaling regulates circuits involved in memory encoding and consolidation.

Methods

Plasmids

Arc-RaPTR (RNA and Protein Translation Reporter): The Arc synaptic activity-responsive element (SARE) and minimal promoter plasmids were obtained from Hiroki Okuno and Haruhiko Bito (University of Tokyo). This promoter sequence was PCR amplified with Mfe1 and Not1 and inserted into the pUB_smHA_KDM5B_MS2 (Addgene plasmid # 81085) lentiviral vector[29] replacing the UbC promoter. The 5' end of this construct contains 10 copies of the HA epitope while the 3' end contains 24 MS2 RNA stem-loops. The Arc ORF was subcloned from pRK5-Arc and the insert was PCR amplified with AsiS1 and Nhe1 and ligated into the pUB_smHA_KDM5B_MS2 backbone.

Arc deletion mutants were generated from pRK5 expression plasmids containing WT rat Arc. Pairs of overlapping primers with homology arms were designed for each deletion, targeting nucleic acid sequences adjacent to the deletion region. Overlap extension PCR reactions were performed using these primers to amplify the full plasmid Arc ORF and backbones minus the targeted deletion sequence to generate an Arc deletion mutant plasmid.

The short-hairpin RNA targeting Arc (TRCN0000108909) was developed by the Broad Institute and purchased from The RNAi Consortium (TRC). The shRNA sequence, AGTCAGTTGAGGCTCAGCAAT, was packaged into the pLKO.1 lentiviral vector.

The ORF of mouse IRSp53 (transcript variant 1, NM_001037755) was amplified by PCR with XhoI and BamHI and ligated into the pLVX lentivirus backbone with or without mRuby. IRSp53^{I403P} gene block was generated by IDT and amplified by PCR with XhoI and BamHI. The insert was then ligated into a pLVX backbone. Rat Arc and Arc$^{\Delta 20\text{-}40}$ was amplified by PCR using XhoI and and XbaI and ligated into a C-terminal pLVX-HiBiT backbone obtained from the Arc-HiBit plasmid. pLVX-eGFP-Cre (plasmid #86805) and pLVX-GFP (plasmid #17448) were purchased from Addgene. IRSp53 I-BAR domain was amplified from the pLVX-IRSp53 plasmid and ligated into a pRK5-myc backbone using SalI and NotI.

Protein purification was carried out using the pGEX-6p1 (GE Healthcare, Little Chalfont, UK) bacterial expression vector. The ORF of mouse IRSp53, IRSp53^{I403P}, and Arc$^{\Delta 20\text{-}40}$ were amplified by PCR from pRK5 vectors with BamH1 and Not1 and ligated into the pGEX-6p1 vector.

Cell Lines

HEK293T cells were purchased from ATCC (#CRL-11268). Cells were maintained at 37°C/5% CO_2 in DMEM media supplemented with 10% fetal bovine serum (FBS) (Thermo Fisher). For transfections, HEK cells were seeded at 40% confluency to either 6-well plates or 10cm dishes. HEK cells were transfected using Polyethylenimine (PEI) (1mg/mL) (Polysciences, cat# 23966-2). 3µg plasmid DNA (6-well dishes) or 8 µg DNA (10 cm dishes) was diluted in OptiMEM whose volume was 10% of the final volume in culture dish. DNA and PEI incubated for 20 min at room temperature (RT) and added to cells to incubate overnight at 37°C/5% CO_2. A full

media change was performed with DMEM supplemented without FBS at 24 hours and media was collected 48 hours post-transfection.

Viral particle production

HEK293T cells (cultured in DMEM + 10% FBS**;** no antibiotics) at 80% confluency in 10cm dishes were co-transfected with 3 µg each of psPax2, pHEF-VSV-G, and pLVX-GFP/eGFP-Cre/pLVX-Arc-HiBiT/pLVX-mIRSp53/pLVX-mIRSp53^{1403P}/Arc$^{\Delta 20\text{-}40}$ -HiBiT or pLKO.1 Arc-shRNA. Plasmid DNA was diluted in OptiMEM and incubated with PEI for 20 min. at RT. Cells underwent a full media change 24 hours post-transfection without FBS and media was collected 48 hours post-transfection. Media was centrifuged at 1000*xg* for 10 min. at 4°C, HEPES was added to a final concentration of 20µM, and then filtered through a 0.45 micron low protein binding filter. Media was then centrifuged at 5000x*g* overnight at 4°C and the viral pellet was resuspended in 1X phosphate buffered saline (PBS). Lentiviral particles were stored at -80°C until transduction.

Mouse models

Wild-type and Arc KO mice (REF) used in these studies were littermates from heterozygous crosses. IRSp53$^{flx/flx}$ mice (a gift from Dr. Eunjoon Kim, Korea Advanced Institute of Science and Technology) were used from homozygous crosses. Both male and female mice were used. Mice were group-housed with littermates of the same sex after weaning (2-5 mice/cage), on a 12:12 hr. day:night cycle, with food and water *ad libitum*.

Rat models

Taconic Biosciences/Cyagen generated the Arc (GenBank accession number: NM_019361.1; Ensembl: ENSRNOG00000043465) KO rats in a Long Evans background by CRISPR/Cas9. gRNAs were created by i*n vitro* transcription (gRNA1: AAGACCTAGACCCATGTATCTGG, gRNA2: AGGCACAGGAACCCCGCCTATGG) and co-injected into fertilized eggs for Arc KO production. Arc KO rats were confirmed by PCR (F1: 5'-GATAGGTTAGCTCTAAGAGAGGCAG-3', R1: 5'-TTGTGTACTCTTGGTAATTCACCTCT-3') with WT allele = 5475 bp and mutant allele = 806 bp. Long Evans Arc KO rats used in this study were from heterozygous crosses. Homozygous pairs were then used for generating primary neuronal cultures. Rats were group-housed with littermates of the same sex after weaning (2-4 rats/cage), on a 12:12 hr. day:night cycle, with food and water *ad libitum*.

Cultured Primary Neurons

Primary neurons were prepared from E18 mouse/rat cortices and hippocampi as previously described[11]. Tissue was dissociated using 0.01% DNase (Sigma Aldrich) and 0.067% papain (Worthington Biochemicals) prior to trituration through glass pipettes to obtain a single-cell suspension. Cells were then plated at 8x10^4 cells/mL in Neurobasal medium (Thermo Fisher) supplemented with 5% FBS (Thermo Fisher), 2% GlutaMAX (Thermo Fisher), 2% SM1 (Thermo Fisher), 1% penicillin and streptomycin (Thermo Fisher) on coverslips (No. 1, Bioscience Tools) coated overnight with 0.2 mg/mL poly-L-lysine (Sigma-Aldrich) in 100 mM Tris-base (pH 8). Neurons were grown at 37°C/5% CO_2 and fed via half-media exchange every 3rd day with astrocyte conditioned

BrainPhys media (StemCell Technologies) supplemented with 1% FBS, 2% SM1 (StemCell Technologies), 500 µM L-Glutamine, and 1% penicillin/streptomycin with DIV5 feeding containing 5µM β-D-arabinofuranoside (Sigma-Aldrich) to limit overgrowth of glial cells. Neurons were grown for 14-16 days *in vitro* (DIV) prior to experiments.

Neuron Transfection

Neurons were transfected after DIV14-15 using lipofectamine 2000 (Thermo Fisher) at a 3:1 ratio when complexed with plasmid DNA. Neurons were transfected over the course of 1 hr. at 37°C in pH 7.2 Minimum Essential Media (Thermo Fisher) supplemented with 2% GlutaMAX, 2% SM1, 15 mM HEPES (Thermo Fisher), 1 mM Sodium Pyruvate (Thermo Fisher), and 33mM Glucose without CO_2. After transfection, the neurons were given 12 hours in growth media at 37°C/5% CO_2 to allow sufficient recovery and expression of the plasmid prior to fixation in 4% formaldehyde (Thermo Fisher) / 4% sucrose (VWR) in 1X PBS for 15 min. at RT. After fixation, neurons were washed with PBS and mounted in Fluoromount G Mounting Medium with or without DAPI (Thermo Fisher) for ICC.

Extracellular Vesicle Purification

Extracellular vesicles (EVs) for synaptic plasticity assays were purified from culture media of DIV15 mouse primary cortical neurons. Media was collected and spun sequentially at 2,000*xg* and 20,000*xg* to remove any cell debris and apoptotic bodies. The clarified media was then concentrated to 0.5 mL using 100kDa Vivaspin protein concentrator spin columns (Cytvia). Concentrated EVs were further fractionated using qEV Gen 2 IZON size exclusion columns (IZON). Void fractions were discarded (3mL) and early fractions that contained EV markers and Arc (fractions 1-4) were used for EV uptake assays at a concentration of 50µg, as determined by nanodrop.

EVs from IRSp53$^{flx/flx}$ mouse cultures were collected from media of five 10cm biochemistry dishes and combined into a single EV preparation isolated by ultracentrifugation over a sucrose cushion. Differential Centrifugation was used to isolate the smallest components released from cells. Low-speed spin (2000*xg* for 10 min.) is performed to remove the largest components in cell culture media followed by a higher-speed spin (20,000*xg* for 20 min.). This was followed by a 134,000*xg* for 70 mins. and then a 33,000*xg* spin on a 20% sucrose cushion for 16 hours to pellet EVs in the 100-120nm size range.

Nanoluciferase assays

Arc-Hibit samples from HEK293T cells were collected 48 hours post transfection and neurons 6 days post transduction. Conditioned media from HEK293T cells or neurons, plated in 6-well dishes were centrifuged at 1000*xg* for 10 minutes and suspended in 5x Passive Lysis buffer (Promega). Each data point represents an individual well. Arc-Hibit signal was identified by complementation with LgBiT (equal volumes) and measurement of Nanoluc-mediated luciferase [JDS1] (Nano-Glo Luciferase Assay, Promega, 565nm) on a microplate reader (SpectraMax iD3).Total Arc in the cell lysate is calculated by dividing the luciferase value of Arc cell lysate by

the % of Arc lysate sample used from total sample collected. Total Arc in media is calculated by dividing the media Arc luciferase value by % of Arc media sample used from total sample calculated. % Arc release is calculated by dividing the total Arc in the media by the sum of the total Arc in the cell lysate and the total Arc in the media.

Arc EV Hibit assay: HEK293T cells were seeded in 10 cm cell culture dishes at ~80% confluency. The cells were transfected with Arc-HiBiT plasmid and either IRSp53 or empty vector plasmids using LipoD293 reagent (SignaGen) according to manufacturer protocol. 48 hours post transfection, conditioned media from Arc-expressing HEK293T cells was harvested and clarified by sequential 300*xg* and 3000*xg* spins. Clarified media was overlayed onto 20-50% w/w sucrose gradients (prepared in serum free DMEM). The gradients were centrifuged in an SW41 rotor at 200,000*xg* for 1hr Fractions were collected from air-gradient interfaces and complemented using LgBiT (Promega, 1:200 dilution) and nanoluc substrate (Promega, 1:200) diluted in 1X passive lysis buffer (Promega). Luminescence of the fractions was measured with a luminometer (Promega, GloMax Explorer). EV-associated HiBiT-Arc was identified in gradient fractions 15-17 as these fractions have a density consistent with the known densities of EVs (1.10-1.15g/mL). Free HiBiT-Arc was identified in fractions 1-8, which comprise the applied conditioned media.

EV nanoparticle tracking analysis

HEK293T cells were seeded in 10 cm cell culture dishes at ~80% confluency. The cells were transfected with Arc-HiBiT plasmid and either IRSp53 or empty vector plasmids using LipoD293 reagent (SignaGen) according to manufacturer protocol. 48 hours post transfection, conditioned media from Arc-expressing HEK293T cells was harvested and clarified by sequential 300*xg* and 3000*xg* spins. The clarified supernatant was applied to 100K Amicon ultrafilters and concentrated ~20-fold. The concentrated media was loaded on IZON qEV original 35 nm size exclusion columns according to manufacturer protocols. Fractions were collected using the IZON automated fraction collector. Fractions were complemented using LgBiT (Promega, 1:200 dilution) and nanoluc substrate (Promega, 1:200) diluted in 1X passive lysis buffer (Promega). Luminescence of the fractions was measured with a luminometer (Promega, GloMax Explorer). EV associated peak fractions were 2-fold serially diluted in PBS and analyzed by nanoparticle tracking analysis (Nanosight NS300, Malvern) to calculate average diameter and concentration of particles. Particle tracks (n = 3) are depicted as averages (line traces) with standard errors of the means depicted as shaded areas.

Western blot

Western blot samples were mixed with 4X Laemmli buffer (40% glycerol, 250 mM Tris, 4% SDS, 50 mM DTT, pH 6.8) and heated at 70°C for 5 min. SDS-PAGE gel electrophoresis was used to separate protein samples. Separated protein samples were transferred to a nitrocellulose membrane (GE Healthcare). Following transfer, membranes were briefly stained with Pierce™ Reversible Total Protein Stain and then destained for total protein imaging. Membranes were blocked in 5% milk + 1X Tris-buffered saline (TBS; 10x: 152.3 mM Tris-HCl, 46.2 mM Tris-base, 1.5 NaCl, pH 7.6) for 30 min. at RT. Membranes were then incubated with in primary antibody in 1X

TBS overnight at 4°C. Membranes were washed 3 x 10 min. in 1X TBS, then incubated with in an HRP-conjugated secondary antibody (Jackson ImmunoResearch) in block for 1 hour. at RT. After 3 x 10 min. washes in 1X TBS, a chemiluminescence kit (Bio-Rad, Hercules, CA) was used to detect the protein bands. Membranes were imaged on an Amersham ImageQuant 800 gel dock (Cytiva). Blots were analyzed using ImageJ/FIJI (National Institutes of Health, Bethesda, MD).

Antibodies

Western blots – Primary antibodies: Arc (1:200; mouse monoclonal, Santa Cruz ; 1:1000; rabbit polyclonal, Synaptic Systems), ALIX (1:500; rabbit polyclonal, custom provided by the Dr. Wesley Sundquist), IRSp53 (1:1000, mouse monoclonal, Abcepta; 1:1000, rabbit polyclonal, Proteintech), PSD-95 (1:2000; mouse monoclonal, US Davis/NIH NeuroMab), GFP (1:1000; mouse monoclonal, Millipore Sigma), myc (1:1000, Sigma Aldrich). All secondary antibodies were used at a dilution of 1:10,000 (HRP-conjugated goat anti-rabbit, goat anti-mouse, goat anti-chicken, Jackson ImmunoResearch).

Immunocytochemistry – Primary antibodies: Arc (1:1000 anti-guinea pig, Synaptic Systems, 1:1000 anti-rabbit, Synaptic Systems, Goettingen, Germany; 1:1000 anti-rabbit, Arc custom antibody, generated by Thermo Fisher); IRSp53 (1:1000 anti-rabbit, Proteintech, Rosemont, IL), MAP2 (1:2000 anti-chicken, ab5392; Abcam), N-terminal GluA1 (1:500 anti-mouse, custom antibody provided by Dr. Richard Huganir, Johns Hopkins Medical School). Secondary antibodies: Alexa Fluor 405, 488, 555, or 647 for the appropriate animal host (1:1000 Thermofisher Scientific).

Immunoprecipitation

Mouse forebrain tissue was dissected out and homogenized in immunoprecipitation (IP) lysis buffer (150 mM NaCl, 50 mM Tris, 3% Triton X-100, pH 7.4), with protease inhibitor cocktail added fresh (Roche). Homogenates were pelleted at 200*xg* for 5 min. at 4°C to remove tissue debris. Supernatants were removed and rotated for 10 min. at 4°C before being pelleted at 10,000*xg* for 10 min. at 4°C to remove insoluble material. Cleared supernatants were removed and a small aliquot was taken as the input, while the remainder was used for the co-IP. Supernatants were immunoprecipitated either with Arc antibody (rabbit polyclonal, custom-made; ThermoFisher) or normal rabbit IgG (Santa Cruz Biotechnology, Santa Cruz, CA) at 2µg/mL overnight at 4°C while rotating. Following antibody incubation, a 10% volume of washed Protein A/G magnetic bead slurry (ThermoFisher Scientific) was added to the antibody/lysate mixture and incubated for 1 hour at 4°C rotating. Bead-antibody mixture was washed 3 times with IP lysis buffer and beads were resuspended in 200 µL IP buffer and then 4X Laemmli buffer was added. Protein was separated from magnetic beads at 70°C for 5 min. and then the beads were isolated using a magnetic bead stand. Input (10% lysate volume) and each of the IgG and Arc antibody elution's were separated by SDS-PAGE on a 10% acrylamide gel and immunoblotted as described above.

Protein Purification

GST-tagged proteins were purified from *Escherichia coli* Rosetta 2 BL21 competent cells as previously described[6]. Starter bacteria cultures were grown overnight at 37°C in LB supplemented with ampicillin and chloramphenicol. Large-scale 500 mL cultures were inoculated with stater cultures in ZY auto-induction media. Large-scale cultures were grown to OD_{600} of 0.6-0.8 at 37°C at 160rpm then shifted to 18°C at 180rpm for 16-20 hours. Cultures were pelleted at 4000x*g* for 15 min at 4°C. Pellets were resuspended in 25 mL of lysis buffer (500 mM NaCl, 50 mM Tris, 5% glycerol, 1 mM DTT, pH 8.0) and flash frozen in liquid nitrogen. Frozen pellets were thawed in 37°C and brought to a final volume of 1g pellet:10 mL lysis buffer, supplemented with DNAse, lysozyme, and complete protease inhibitor cocktail (Roche). Resuspended lysates were sonicated for 6 x 45s pulses at 90% duty cycle and pelleted for 75 min. at 21,000x*g*. Cleared supernatants were incubated with pre equilibrated GST Sepharose 4B affinity resin in a gravity flow column overnight at 4°C. GST-bound protein was washed twice with 20 resin bed volumes of lysis buffer and re-equilibrated in TBS (150 mM NaCl, 50 mM Tris, 1 mM EDTA, 1mM DTT, pH 7.2) at RT, and cleaved from GST resin overnight at 4°C with PreScission Protease (GE Healthcare). GST was affinity purified as described above and eluted using 15 mM reduced L-gluathione, 10 mM Tris, pH 7.4 at RT.

GST-pulldowns

Purified proteins were either left fused to the GST tag or were cleaved using PreScission protease. GST-tagged proteins were incubated with each respective cleaved protein overnight at 4°C. The following day, a column was washed several times with TBS and the incubated proteins were added to the column. PreScission protease (L-reduced glutathione (20mM, pH 8.0)) was added to the column and incubated with the proteins for 20 min. The cleaved protein complexes were eluted from the column and prepared for SDS-PAGE and western blot.

Arc Capsid Assembly Assay

GST cleaved purified Arc and IRSp53 protein elutes were concentrated in Vivaspin 30kDa MWCO ultrafiltration spin columns (Cytvia) to 2.5 mL and protein concentration was measured by nanodrop. Equal concentrations of Arc, IRSp53, or Arc and IRSp53 incubated in a 1:1 ratio for 2 hours in TBS and were then run on a Superdex 200pg HiLoad 16/600 size exclusion column in TBS. Peak fractions, determined by chromatogram and Coomassie staining, were pooled and concentrated. Following size exclusion, negative stain EM grids were prepared for each sample at 0.5mg/mL and capsid formation was quantified by manual counting of 15 images/grid.

Negative Stain EM

For all negative stain EM samples, copper 200-mesh grids (Electron Microscopy Sciences) were glow discharged for 25 s in a vacuum chamber at 30 mA. 3.5 µL of sample was applied to the grid for 45s. Grids were washed 2 x 5 s with 30µL water droplets, followed by one wash with 1% uranyl acetate (UA) on parafilm. Excess water/UA was removed from the grid with filter paper and a final droplet of UA was added to grids for 30s. Excess UA was removed, and grids were air dried for 30s. Imaging was performed using either an FEI T12, FEI Tecnai Spirit

microscope at 120 kV or a JEOL-JEM 1400 electron microscope. For each experiment, 15 images were taken of each sample from a stereotyped pattern of grid squares. Arc capsids between 30-50 nm were manually counted using ImageJ/FIJI.

Capsid Binding Assay

Arc proteins were purified as described above and they were subjected to Superdex 200 column in the presence of 500 mM phosphate buffer. Early fractions were collected, and capsid assembly was confirmed by TEM images. HEK293Ts were transfected using PEI to overexpress IRSp53. The cells were lysed by passive lysis buffer containing a protease inhibitor cocktail. The cell lysate was incubated with *in vitro* assembled Arc capsids for 1 hour at 4°C. The mixture was pelleted by ultracentrifugation at 21,000*xg* for 15 min. The pellets were washed with 500 mM phosphate buffer 3x, and they were resuspended in loading buffer for western blot analysis. The supernatant fractions were collected for further analysis. Pellet and input fractions (10x diluted) are analyzed by SDS-PAGE and immunoblot.

GluA1 Surface-Labeling

Primary hippocampal mouse neurons were surface labeled for GluA1 with a live antibody feeding assay. Living DIV14-16 neurons were washed briefly with cooled (10°C) neuronal incubation media (NIM) (1X MEM, 2% GlutaMax, 10mM HEPES, 1 mM sodium pyruvate, 33 mM glucose, 2% SM1 supplement, pH 7.2, filter sterilize) and then incubated in GluA1-NT mouse monoclonal antibody (1:500) (custom provided by Richard Huganir, clone 4.9D) in NIM at 10°C for 20 min. Neurons were washed in NIM and then fixed in 4% formaldehyde prior to immunocytochemistry.

Chemical LTP and LTD

Chemical LTP (cLTP) was induced by incubating neurons in tetrodotoxin (TTX) (1:1000) overnight. The following day, neurons were washed 3 times with glia-conditioned BrainPhys (GCBP) and then given a 5 min. 200μM glycine pulse made in GCBP. Neurons were washed an additional 3 times with GCBP and allowed to recover for 30 min (GluA1 surface-labeled neurons) or 2 hours (Arc release), prior to experimentation. Chemical LTD (cLTD) was induced by washing neurons 3 times with GCBP prior to a 5 min. 50μM DHPG pulse. Neurons were washed 3 times and recovered for 30 min.

Immunocytochemistry

Neurons were washed once with 4% sucrose/1X PBS at 37°C and then fixed for 15 min. with 4% sucrose/4% formaldehyde (ThermoFisher Scientific) in 1X PBS. Neurons were washed 3 x 5 min. with 1X PBS, permeabilized for 10 min. with 0.2% Triton X-100 (Amresco, Solon, OH) in 1X PBS, and blocked in 5% bovine serum albumin (BSA) in 1X PBS for 30 min. at RT. Neurons were incubated in primary antibody diluted in block for 1 hour at RT, washed 3 x 5 min. in 1X PBS, and incubated in secondary antibody diluted in block for 1 hour at RT. Neurons on coverslips were mounted on glass slides in Fluoromount (ThermoFisher Scientific) and dried overnight at RT.

Cell Imaging and Analysis

Imaging coverslips were imaged on a 60x/1.4NA oil objective on a Nikon Eclipse Ti2-E inverted confocal microscope and images were analyzed using ImageJ/FIJI software. Neurons were selected for analysis by looking at MAP2 dendritic staining for cell health. Each experimental group was thresholded based on no primary controls and the brightest immunofluorescent sample was used to determine the image acquisition settings in each experiment. All acquired images from a single experiment were based upon these exact same settings.

Analysis of Arc and IRSp53 protein expression – During image analysis images were thresholded (to minimize background fluorescence and normalize the linear range) to the brightest immunofluorescence in an experiment. This threshold was then applied to all other images. Raw integrated density of three 20 µm tertiary dendritic segments/neuron were measured for each image. This value was divided by the area of the dendritic segment, determined by MAP2. The control group in each experiment was set to "1", and the raw integrated density divided by area of all other groups were normalized to this and displayed ± SEM. For representative images looking at surface GluA1 staining, the Inferno look-up table (LUT) in ImageJ/FIJI was used.

Analysis of Arc and IRSp53 colocalization – An algorithm was designed using the surface feature function in Imaris v8.4.1 (Bitplane) to generate surfaces around Arc signal and the maximum fluorescence intensity of IRSp53 present within these individual Arc surfaces was determined. The algorithm was applied to all images within the same experiment. Background levels of IRSp53 fluorescent intensity was determined and used to calculate the percentage that colocalized with Arc and the percentage that did not colocalize. The same procedure was performed for all experimental conditions and replicates.

Live-cell imaging and analysis

Live-cell imaging was performed using a Leica Yokogawa CSU-W1 spinning disk confocal microscope with a Leica Plan-Apochromat 63x/1.4 NA oil objective and iXon Life 888 EMCCD camera. For all live-cell images neurons were maintained at 37°C/5% CO_2, with a stage top incubator. DIV 15-16 primary cultured hippocampal neurons were used for all live-cell imaging experiments. Neurons were transfected at DIV14-15 with 1µg of Arc-RaPTR, HA-GFP Frankenbody, MS2-miRFP703 coat protein, or in combination with a C-terminally tagged IRSp53-mRuby. Transfected neurons were immediately treated with TTX (1:1000) and recovered overnight at 37°C/5% CO_2. The following day the transfected neurons were imaged for 10-15 min. while in TTX. Neurons were washed to remove residual TTX and then incubated in 200 mM glycine for 5 min. Neurons were washed again and incubated in glia conditioned media for the remaining image acquisition. Prior to imaging after cLTP induction, image drift was accounted for by resetting image coordinates.

Images were analyzed using ImageJ/FIJI. Images were run through a custom macro to threshold and remove background fluorescence for each individual experiment. Particle movement/velocity was tracked manually using FIJI plugin MTrackJ on raw videos. Kymographs were generated using the KymographClear/KymographDirect plugin and software package. Raw integrated density (sum of the region of interest (ROI) pixel intensity/area) of

the entire image was measured during the time course. An average raw integrated density of the 5 min. immediately after the glycine pulse and the last 5 min. of the image acquisition was calculated for measurements of change of relative Arc expression. Outliers were identified and removed using Prism (GraphPad).

Statistical analysis

One and two-way ANOVAs with repeated measures (with *post hoc* Sidak's tests), paired t-tests or two-tailed unpaired *t-tests* were performed using GraphPad Prism (GraphPad Software, San Diego, CA). For all statistical analysis significance was set at $p < 0.05$ and all data shown are representative of at least two biologic replicates.

Acknowledgements

We thank Dr.Hiroki Okuno and Dr. Haruhiko Bito (Tokyo University) for gifting the Arc synaptic activity-responsive element (SARE) and minimal promoter plasmids. We thank Dr. Richard Huganir (Johns Hopkins Medical School) for providing the N-terminal GluA1 antibodies. We thank Dr Eunjoon Kim (Korea Advanced Institute of Science and Technology) for gifting us with the IRSp53$^{flx/flx}$ mice. The authors would like to acknowledge David Rademacher and the Imaging Core at the Stritch School of Medicine for assistance in generating electron micrographs of Hibit-tagged Arc capsids. We thank all members of the Shepherd, past and present, for technical support and help.

E.M.C, T.G., and J.D.S were supported by a NIH Director's Office Transformative Research Award (R01 NS115716). J.D.S was supported by the Chan-Zuckerberg Initiative Ben Barres Early Acceleration Award and the Jon M. Huntsman Presidential Endowed Chair fund.

Author Contributions

A.R performed the *in vivo* and *in vitro* immunoprecipitations, Arc-Hibit assays in HEK293T cells and primary cultured neurons, immunocytochemistry, molecular biology, and confocal microscopy. K.S performed protein purification, electron microscopy, live-cell imaging, molecular biology, EV isolation, immunocytochemistry, and confocal microscopy. J.E performed the IRSp53$^{flx/flx}$ primary neuron EV collections and biochemistry. S.K conducted the capsid binding assay. T.K performed the equilibrium density gradient isolation and nanoparticle tracking analysis on Arc-containing EVs. M.T conducted the IRSp53 GST-pulldown. T.S and A.S generated the mouse and rat primary cultured neurons. K.L designed and cloned the Arc-RaPTR reporter. A.D performed the Arc and IRSp53 colocalization analysis. A.R, K.S, M.H, J.E, S.K, T.K, K.L, A.D, T.G E.C, and J.D.S conceived and designed experiments. A.R, K.S, and J.D.S wrote the manuscript; all authors discussed results. T.G, E.C, and J.D obtained funding for the project.

References

1. Yap, E.L., and Greenberg, M.E. (2018). Activity-Regulated Transcription: Bridging the Gap between Neural Activity and Behavior. Neuron *100*, 330-348. 10.1016/j.neuron.2018.10.013.
2. Plath, N., Ohana, O., Dammermann, B., Errington, M.L., Schmitz, D., Gross, C., Mao, X., Engelsberg, A., Mahlke, C., Welzl, H., et al. (2006). Arc/Arg3.1 Is Essential for the Consolidation of Synaptic Plasticity and Memories. Neuron *52*, 437-444. 10.1016/j.neuron.2006.08.024.
3. Shepherd, J.D., and Bear, M.F. (2011). New views of Arc, a master regulator of synaptic plasticity. Nat Neurosci *14*, 279-284. 10.1038/nn.2708.
4. Ashley, J., Cordy, B., Lucia, D., Fradkin, L.G., Budnik, V., and Thomson, T. (2018). Retrovirus-like Gag Protein Arc1 Binds RNA and Traffics across Synaptic Boutons. Cell *172*, 262-274 e211. 10.1016/j.cell.2017.12.022.
5. Hantak, M.P., Einstein, J., Kearns, R.B., and Shepherd, J.D. (2021). Intercellular Communication in the Nervous System Goes Viral. Trends Neurosci *44*, 248-259. 10.1016/j.tins.2020.12.003.
6. Pastuzyn, E.D., Day, C.E., Kearns, R.B., Kyrke-Smith, M., Taibi, A.V., McCormick, J., Yoder, N., Belnap, D.M., Erlendsson, S., Morado, D.R., et al. (2018). The Neuronal Gene Arc Encodes a Repurposed Retrotransposon Gag Protein that Mediates Intercellular RNA Transfer. Cell *172*, 275-288 e218. 10.1016/j.cell.2017.12.024.
7. Zhang, W., Wu, J., Ward, Matthew D., Yang, S., Chuang, Y.-A., Xiao, M., Li, R., Leahy, Daniel J., and Worley, Paul F. (2015). Structural Basis of Arc Binding to Synaptic Proteins: Implications for Cognitive Disease. Neuron *86*, 490-500. 10.1016/j.neuron.2015.03.030.
8. Shepherd, J.D., and Huganir, R.L. (2007). The cell biology of synaptic plasticity: AMPA receptor trafficking. Annu Rev Cell Dev Biol *23*, 613-643. 10.1146/annurev.cellbio.23.090506.123516.
9. Chowdhury, S., Shepherd, J.D., Okuno, H., Lyford, G., Petralia, R.S., Plath, N., Kuhl, D., Huganir, R.L., and Worley, P.F. (2006). Arc/Arg3.1 interacts with the endocytic machinery to regulate AMPA receptor trafficking. Neuron *52*, 445-459. 10.1016/j.neuron.2006.08.033.
10. Gao, M., Sossa, K., Song, L., Errington, L., Cummings, L., Hwang, H., Kuhl, D., Worley, P., and Lee, H.K. (2010). A specific requirement of Arc/Arg3.1 for visual experience-induced homeostatic synaptic plasticity in mouse primary visual cortex. J Neurosci *30*, 7168-7178. 10.1523/JNEUROSCI.1067-10.2010.
11. Shepherd, J.D., Rumbaugh, G., Wu, J., Chowdhury, S., Plath, N., Kuhl, D., Huganir, R.L., and Worley, P.F. (2006). Arc/Arg3.1 mediates homeostatic synaptic scaling of AMPA receptors. Neuron *52*, 475-484. 10.1016/j.neuron.2006.08.034.
12. Steward, O., Wallace, C.S., Lyford, G.L., and Worley, P.F. (1998). Synaptic activation causes the mRNA for the IEG Arc to localize selectively near activated postsynaptic sites on dendrites. Neuron *21*, 741-751. 10.1016/s0896-6273(00)80591-7.
13. Kyrke-Smith, M., Volk, L.J., Cooke, S.F., Bear, M.F., Huganir, R.L., and Shepherd, J.D. (2021). The Immediate Early Gene Arc Is Not Required for Hippocampal Long-Term Potentiation. J Neurosci *41*, 4202-4211. 10.1523/JNEUROSCI.0008-20.2021.

14. Budnik, V., Ruiz-Cañada, C., and Wendler, F. (2016). Extracellular vesicles round off communication in the nervous system. Nature Reviews Neuroscience *17*, 160-172. 10.1038/nrn.2015.29.

15. Faure, J., Lachenal, G., Court, M., Hirrlinger, J., Chatellard-Causse, C., Blot, B., Grange, J., Schoehn, G., Goldberg, Y., Boyer, V., et al. (2006). Exosomes are released by cultured cortical neurones. Mol Cell Neurosci *31*, 642-648. 10.1016/j.mcn.2005.12.003.

16. Yeh, T.C., Ogawa, W., Danielsen, A.G., and Roth, R.A. (1996). Characterization and cloning of a 58/53-kDa substrate of the insulin receptor tyrosine kinase. J Biol Chem *271*, 2921-2928. 10.1074/jbc.271.6.2921.

17. Inamdar, K., Tsai, F.C., Dibsy, R., de Poret, A., Manzi, J., Merida, P., Muller, R., Lappalainen, P., Roingeard, P., Mak, J., et al. (2021). Full assembly of HIV-1 particles requires assistance of the membrane curvature factor IRSp53. Elife *10*. 10.7554/eLife.67321.

18. Thomas, A., Mariani-Floderer, C., Lopez-Huertas, M.R., Gros, N., Hamard-Peron, E., Favard, C., Ohlmann, T., Alcami, J., and Muriaux, D. (2015). Involvement of the Rac1-IRSp53-Wave2-Arp2/3 Signaling Pathway in HIV-1 Gag Particle Release in CD4 T Cells. J Virol *89*, 8162-8181. 10.1128/JVI.00469-15.

19. Scita, G., Confalonieri, S., Lappalainen, P., and Suetsugu, S. (2008). IRSp53: crossing the road of membrane and actin dynamics in the formation of membrane protrusions. Trends Cell Biol *18*, 52-60. 10.1016/j.tcb.2007.12.002.

20. Chen, C.J., Shih, C.H., Chang, Y.J., Hong, S.J., Li, T.N., Wang, L.H., and Chen, L. (2015). SH2B1 and IRSp53 proteins promote the formation of dendrites and dendritic branches. J Biol Chem *290*, 6010-6021. 10.1074/jbc.M114.603795.

21. Kang, J., Park, H., and Kim, E. (2016). IRSp53/BAIAP2 in dendritic spine development, NMDA receptor regulation, and psychiatric disorders. Neuropharmacology *100*, 27-39. 10.1016/j.neuropharm.2015.06.019.

22. de Poret, A., Dibsy, R., Merida, P., Trausch, A., Inamdar, K., and Muriaux, D. (2022). Extracellular vesicles containing the I-BAR protein IRSp53 are released from the cell plasma membrane in an Arp2/3 dependent manner. Biol Cell *114*, 259-275. 10.1111/boc.202100095.

23. Dosemeci, A., Burch, A., Loo, H., Toy, D., and Tao-Cheng, J.H. (2017). IRSp53 accumulates at the postsynaptic density under excitatory conditions. PLoS One *12*, e0190250. 10.1371/journal.pone.0190250.

24. Burette, A.C., Park, H., and Weinberg, R.J. (2014). Postsynaptic distribution of IRSp53 in spiny excitatory and inhibitory neurons. J Comp Neurol *522*, 2164-2178. 10.1002/cne.23526.

25. Fernandez, E., Collins, M.O., Frank, R.A.W., Zhu, F., Kopanitsa, M.V., Nithianantharajah, J., Lempriere, S.A., Fricker, D., Elsegood, K.A., McLaughlin, C.L., et al. (2017). Arc Requires PSD95 for Assembly into Postsynaptic Complexes Involved with Neural Dysfunction and Intelligence. Cell Rep *21*, 679-691. 10.1016/j.celrep.2017.09.045.

26. Dixon, A.S., Schwinn, M.K., Hall, M.P., Zimmerman, K., Otto, P., Lubben, T.H., Butler, B.L., Binkowski, B.F., Machleidt, T., Kirkland, T.A., et al. (2016). NanoLuc Complementation Reporter Optimized for

Accurate Measurement of Protein Interactions in Cells. ACS Chem Biol *11*, 400-408. 10.1021/acschembio.5b00753.

27. Robens, J.M., Yeow-Fong, L., Ng, E., Hall, C., and Manser, E. (2010). Regulation of IRSp53-dependent filopodial dynamics by antagonism between 14-3-3 binding and SH3-mediated localization. Mol Cell Biol *30*, 829-844. 10.1128/MCB.01574-08.
28. Chung, W., Choi, S.Y., Lee, E., Park, H., Kang, J., Park, H., Choi, Y., Lee, D., Park, S.G., Kim, R., et al. (2015). Social deficits in IRSp53 mutant mice improved by NMDAR and mGluR5 suppression. Nat Neurosci *18*, 435-443. 10.1038/nn.3927.
29. Morisaki, T., Lyon, K., DeLuca, K.F., DeLuca, J.G., English, B.P., Zhang, Z., Lavis, L.D., Grimm, J.B., Viswanathan, S., Looger, L.L., et al. (2016). Real-time quantification of single RNA translation dynamics in living cells. Science *352*, 1425-1429. 10.1126/science.aaf0899.
30. Kawashima, T., Okuno, H., Nonaka, M., Adachi-Morishima, A., Kyo, N., Okamura, M., Takemoto-Kimura, S., Worley, P.F., and Bito, H. (2009). Synaptic activity-responsive element in the Arc/Arg3.1 promoter essential for synapse-to-nucleus signaling in activated neurons. Proc Natl Acad Sci U S A *106*, 316-321. 10.1073/pnas.0806518106.
31. Dick, R.A., Zadrozny, K.K., Xu, C., Schur, F.K.M., Lyddon, T.D., Ricana, C.L., Wagner, J.M., Perilla, J.R., Ganser-Pornillos, B.K., Johnson, M.C., et al. (2018). Inositol phosphates are assembly co-factors for HIV-1. Nature *560*, 509-512. 10.1038/s41586-018-0396-4.
32. Muriaux, D., and Darlix, J.L. (2010). Properties and functions of the nucleocapsid protein in virus assembly. RNA Biol *7*, 744-753. 10.4161/rna.7.6.14065.
33. Erlendsson, S., Morado, D.R., Cullen, H.B., Feschotte, C., Shepherd, J.D., and Briggs, J.A.G. (2020). Structures of virus-like capsids formed by the Drosophila neuronal Arc proteins. Nat Neurosci *23*, 172-175. 10.1038/s41593-019-0569-y.
34. Cai, Q., Qiao, L., Wang, M., He, B., Lin, F.M., Palmquist, J., Huang, S.D., and Jin, H. (2018). Plants send small RNAs in extracellular vesicles to fungal pathogen to silence virulence genes. Science *360*, 1126-1129. 10.1126/science.aar4142.
35. Zappulli, V., Friis, K.P., Fitzpatrick, Z., Maguire, C.A., and Breakefield, X.O. (2016). Extracellular vesicles and intercellular communication within the nervous system. J Clin Invest *126*, 1198-1207. 10.1172/JCI81134.
36. Graykowski, D.R., Wang, Y.Z., Upadhyay, A., and Savas, J.N. (2020). The Dichotomous Role of Extracellular Vesicles in the Central Nervous System. iScience *23*, 101456. 10.1016/j.isci.2020.101456.
37. Vilcaes, A.A., Chanaday, N.L., and Kavalali, E.T. (2021). Interneuronal exchange and functional integration of synaptobrevin via extracellular vesicles. Neuron *109*, 971-983 e975. 10.1016/j.neuron.2021.01.007.
38. Lee, S.H., Shin, S.M., Zhong, P., Kim, H.T., Kim, D.I., Kim, J.M., Heo, W.D., Kim, D.W., Yeo, C.Y., Kim, C.H., and Liu, Q.S. (2018). Reciprocal control of excitatory synapse numbers by Wnt and Wnt inhibitor PRR7 secreted on exosomes. Nat Commun *9*, 3434. 10.1038/s41467-018-05858-2.

39. Sharma, P., Mesci, P., Carromeu, C., McClatchy, D.R., Schiapparelli, L., Yates, J.R., 3rd, Muotri, A.R., and Cline, H.T. (2019). Exosomes regulate neurogenesis and circuit assembly. Proc Natl Acad Sci U S A *116*, 16086-16094. 10.1073/pnas.1902513116.

40. Bobsin, K., and Kreienkamp, H.J. (2016). Severe learning deficits of IRSp53 mutant mice are caused by altered NMDA receptor-dependent signal transduction. J Neurochem *136*, 752-763. 10.1111/jnc.13428.

41. Choi, J., Ko, J., Racz, B., Burette, A., Lee, J.R., Kim, S., Na, M., Lee, H.W., Kim, K., Weinberg, R.J., and Kim, E. (2005). Regulation of dendritic spine morphogenesis by insulin receptor substrate 53, a downstream effector of Rac1 and Cdc42 small GTPases. J Neurosci *25*, 869-879. 10.1523/JNEUROSCI.3212-04.2005.

42. Kim, Y., Noh, Y.W., Kim, K., Yang, E., Kim, H., and Kim, E. (2020). IRSp53 Deletion in Glutamatergic and GABAergic Neurons and in Male and Female Mice Leads to Distinct Electrophysiological and Behavioral Phenotypes. Front Cell Neurosci *14*, 23. 10.3389/fncel.2020.00023.

43. Nishimura, T., Oyama, T., Hu, H.T., Fujioka, T., Hanawa-Suetsugu, K., Ikeda, K., Yamada, S., Kawana, H., Saigusa, D., Ikeda, H., et al. (2021). Filopodium-derived vesicles produced by MIM enhance the migration of recipient cells. Dev Cell *56*, 842-859 e848. 10.1016/j.devcel.2021.02.029.

44. D'Angelo, G., Raposo, G., Nishimura, T., and Suetsugu, S. (2023). Protrusion-derived vesicles: new subtype of EVs? Nat Rev Mol Cell Biol *24*, 81-82. 10.1038/s41580-022-00555-x.

45. Ying, S.W., Futter, M., Rosenblum, K., Webber, M.J., Hunt, S.P., Bliss, T.V., and Bramham, C.R. (2002). Brain-derived neurotrophic factor induces long-term potentiation in intact adult hippocampus: requirement for ERK activation coupled to CREB and upregulation of Arc synthesis. J Neurosci *22*, 1532-1540. 10.1523/JNEUROSCI.22-05-01532.2002.

46. Messaoudi, E., Kanhema, T., Soule, J., Tiron, A., Dagyte, G., da Silva, B., and Bramham, C.R. (2007). Sustained Arc/Arg3.1 synthesis controls long-term potentiation consolidation through regulation of local actin polymerization in the dentate gyrus in vivo. J Neurosci *27*, 10445-10455. 10.1523/JNEUROSCI.2883-07.2007.

47. Guzowski, J.F., Lyford, G.L., Stevenson, G.D., Houston, F.P., McGaugh, J.L., Worley, P.F., and Barnes, C.A. (2000). Inhibition of activity-dependent arc protein expression in the rat hippocampus impairs the maintenance of long-term potentiation and the consolidation of long-term memory. J Neurosci *20*, 3993-4001. 10.1523/JNEUROSCI.20-11-03993.2000.

48. Rial Verde, E.M., Lee-Osbourne, J., Worley, P.F., Malinow, R., and Cline, H.T. (2006). Increased expression of the immediate-early gene arc/arg3.1 reduces AMPA receptor-mediated synaptic transmission. Neuron *52*, 461-474. 10.1016/j.neuron.2006.09.031.

49. Wall, M.J., Collins, D.R., Chery, S.L., Allen, Z.D., Pastuzyn, E.D., George, A.J., Nikolova, V.D., Moy, S.S., Philpot, B.D., Shepherd, J.D., et al. (2018). The Temporal Dynamics of Arc Expression Regulate Cognitive Flexibility. Neuron *98*, 1124-1132 e1127. 10.1016/j.neuron.2018.05.012.

50. Wall, M.J., and Correa, S.A.L. (2018). The mechanistic link between Arc/Arg3.1 expression and AMPA receptor endocytosis. Semin Cell Dev Biol *77*, 17-24. 10.1016/j.semcdb.2017.09.005.

51. Nielsen, L.D., Pedersen, C.P., Erlendsson, S., and Teilum, K. (2019). The Capsid Domain of Arc Changes Its Oligomerization Propensity through Direct Interaction with the NMDA Receptor. Structure *27*, 1071-1081 e1075. 10.1016/j.str.2019.04.001.

52. Jenks, K.R., and Shepherd, J.D. (2020). Experience-Dependent Development and Maintenance of Binocular Neurons in the Mouse Visual Cortex. Cell Rep *30*, 1982-1994 e1984. 10.1016/j.celrep.2020.01.031.

53. McCurry, C.L., Shepherd, J.D., Tropea, D., Wang, K.H., Bear, M.F., and Sur, M. (2010). Loss of Arc renders the visual cortex impervious to the effects of sensory experience or deprivation. Nat Neurosci *13*, 450-457. 10.1038/nn.2508.

54. Das, S., Lituma, P.J., Castillo, P.E., and Singer, R.H. (2023). Maintenance of a short-lived protein required for long-term memory involves cycles of transcription and local translation. Neuron *111*, 2051-2064 e2056. 10.1016/j.neuron.2023.04.005.

55. Abel, T., and Lattal, K.M. (2001). Molecular mechanisms of memory acquisition, consolidation and retrieval. Curr Opin Neurobiol *11*, 180-187. 10.1016/s0959-4388(00)00194-x.

56. Mau, W., Hasselmo, M.E., and Cai, D.J. (2020). The brain in motion: How ensemble fluidity drives memory-updating and flexibility. Elife *9*. 10.7554/eLife.63550.

57. Okuno, H., Akashi, K., Ishii, Y., Yagishita-Kyo, N., Suzuki, K., Nonaka, M., Kawashima, T., Fujii, H., Takemoto-Kimura, S., Abe, M., et al. (2012). Inverse synaptic tagging of inactive synapses via dynamic interaction of Arc/Arg3.1 with CaMKIIbeta. Cell *149*, 886-898. 10.1016/j.cell.2012.02.062.

58. Fromer, M., Pocklington, A.J., Kavanagh, D.H., Williams, H.J., Dwyer, S., Gormley, P., Georgieva, L., Rees, E., Palta, P., Ruderfer, D.M., et al. (2014). De novo mutations in schizophrenia implicate synaptic networks. Nature *506*, 179-184. 10.1038/nature12929.

59. Toma, C., Hervas, A., Balmana, N., Vilella, E., Aguilera, F., Cusco, I., del Campo, M., Caballero, R., De Diego-Otero, Y., Ribases, M., et al. (2011). Association study of six candidate genes asymmetrically expressed in the two cerebral hemispheres suggests the involvement of BAIAP2 in autism. J Psychiatr Res *45*, 280-282. 10.1016/j.jpsychires.2010.09.001.